UNIVERSITY OF CALIFORNIA SAN DIEGO

ELECTRICAL IMPEDANCE ACROSS THE OSTEOCHONDRAL INTERFACE: VARIATION WITH NORMAL SKELETAL MATURATION AND OSTEOARTHRITIS

A Thesis submitted in partial satisfaction of the requirements

for the degree Master of Science

in

Bioengineering

by

Caroline G Bullard

Committee in charge:

Professor Robert Sah, Chair
Professor Koichi Masuda
Professor Bruce Wheeler

2022

The Thesis of Caroline G Bullard is approved, and it is acceptable in quality and form for publication on microfilm and electronically.

University of California San Diego

2022

TABLE OF CONTENTS

THESIS APPROVAL PAGE……... iii

TABLE OF CONTENTS iv

LIST OF FIGURES..... vi

LIST OF TABLES vii

ACKNOWLEDGEMENTS viii

VITA ix

ABSTRACT OF THE THESIS x

CHAPTER 1..... 1

1.1 General Introduction To The Thesis 1
1.2. Glossary Of Terms 4
1.3 Articular Cartilage Structure And Function..... 6
1.4 Subchondral Plate Structure And Function..... 7
1.5 Trabecular Bone Structure And Function 8
1.6 Osteochondral Changes During Development..... 10
1.7 Osteochondral Changes During Progression Of Osteoarthritis 12
1.8 Theoretical Calculations Of Solution Impedance 15
1.9 Electrical Properties Of Osteochondral Tissues..... 20
1.10 References..... 23
CHAPTER 2..... 26

2.1 Abstract 26
2.2 Introduction..... 28
2.3 Equation Derivations For Reservoir Configurations..... 32
2.4 Materials And Methods..... 35
2.5 Results..... 40
2.6 Discussion 57
2.7 Acknowledgements..... 61
2.7 References..... 62

CHAPTER 3 64
3.1 Summary Of Findings 64
3.2 Discussion 64
3.3 Future Work 65
APPENDIX 66

LIST OF FIGURES

Figure 1.1: Schematic depicting the osteochondral interface, including the articular cartilage (AC), subchondral slate (ScP) composed of the subchondral bone plate (ScBP) and calcified cartilage (CC), and underlying trabecular (cancellous) bone (TB)……... 9

Figure 1.2: Changes to the osteochondral interface in a rabbit trochlea with normal skeletal maturation …… 11

Figure 1.3: Schematic depicting relevant differences between a healthy joint and an osteoarthritic human joint ……..... 14

Figure 1.4: Contributions to resistance in a cylindrical sample and reservoir set up……. 17

Figure 2.1: Schematic of the different reservoir system configurations implemented for impedance measurements..... 31

Figure 2.2: Schematic of dimensions of arbitrary osteochondral core…….43

Figure 2.3: Effect of centrifugation for marrow removal on impedance across immature bovine osteochondral cores……. 44

Figure 2.4: Representative (A-D) gross and (E, F) μCT images of (A, C, D) bAdult and (B, D, F) bCalf osteochondral cores. (A, B) show whole, intact osteochondral cores. (C, D) show cores post-sectioning, and (E, F) show the osteochondral interface of representative whole cores with 5x zoom…….48

Figure 2.5: Effect of maturation on impedance across bovine OC at 1khz……. 49

Figure 2.6: Representative (A-D) gross and (E, F) μCT images of (A, C, D) normal (NL-hAdult) and (B, D, F) osteoarthritic (OA-hAdult) osteochondral cores. (A, B) show whole, intact osteochondral cores. (C, D) show cores post-sectioning, and (E, F) show the osteochondral interface of representative whole cores with 5X zoom……. 54

Figure 2.7: Effect of degeneration with Osteoarthritis on impedance across human OC core at 1kHz ……55

LIST OF TABLES

Table 1.1: Dimensions of Reservoir System 2.0 relevant for theoretical impedance, resistivity calculations ……. 18

Table 1.2: Theoretical Resistivity for PBS (1x, 1/10x)…… 19

Table 2.1: Human Tissue Information ……..……37

Table 2.2: Dimensions of osteochondral cores by subcomponent……... 42

Table 2.3: Raw and Adjusted Summary Data for Impedance Measurements of Bovine Osteochondral Cores in high and low concentration PBS at 1kHz. Data are shown as mean ± SD. P-values denote relevant hypothesis tests comparing between groups ($p<0.05$)……...47

Table 2.4: Calculated resistivities for bovine tissue measurements in high and low concentration PBS. Results shown were calculated from raw data collected at 1kHz. Data are shown as mean ± SD. [Ω·m]……. 50

Table 2.5: Raw and Adjusted Summary Data for Impedance measurements of Human Osteochondral Cores in high and low concentration PBS at 1kHz. Data are shown as mean ± SD. P-values denote relevant hypothesis tests between groups ($p<0.05$)…… 53

Table 2.6: Calculated resistivities for human tissue measurements at 1kHz in high and low concentration PBS.. Data are shown as mean ± SD [Ω ·m] …… 56

ACKNOWLEDGEMENTS

I would like to acknowledge Professor Robert L. Sah as the chair of my committee and for providing guidance and encouragement throughout the course of my research. I would also like to thank the Albert C Chen and Van W Wong for their assistance in the project.

Chapter 2, in part is currently being prepared for submission for publication of the material. Bullard, Caroline; Wong, Van W; Chen, Albert C.; Masuda, Koichi; Bugbee, William D; Sah, Robert L. Thesis author was the primary investigator and author of this material.

I would also like to thank my family for their endless support, I could not have done it without them.

VITA

2020	Bachelor of Science, Bioengineering University of the Pacific, Stockton, California
2020-2022	Graduate Student Researcher Cartilage Tissue Engineering Laboratory University of California San Diego, La Jolla, California
2022	Master of Science in Bioengineering, University of California San Diego, La Jolla, California

ABSTRACT OF THE THESIS

ELECTRICAL IMPEDANCE ACROSS THE OSTEOCHONDRAL INTERFACE: VARIATION WITH NORMAL SKELETAL MATURATION AND OSTEOARTHRITIS

by

Caroline G Bullard

Master of Science in Bioengineering

University of California San Diego, 2022

Professor Robert L Sah, Chair

Osteochondral cores (OC) consist of articular cartilage, trabecular bone, and the subchondral plate (ScP). Subcomponents change during maturation and degeneration with osteoarthritis. The goal of this thesis was to determine if OC electrical impedance and resistivity differ with tissue maturation or degeneration and if these differences are primarily due to the ScP.

(1) By performing impedance measurements across tubes of varying lengths, resistivity of PBS (1x, 1/10x) was established. (2) The impedance (Z) of immature bovine OC was reduced by 30% after marrow removal via centrifugation. (3) Bovine ScP maturation affected Z^{OC}. In 1x PBS, bCalf-Z^{OC} was 8% of bAdult. ScP+TB accounted for 51% of the summed subcomponent impedances in bCalf and 76% in bAdult. Z^{ScP+TB}-bCalf was 5% of bAdult. After partial and complete equilibration in 1/10x PBS, Z^{ScP+TB} was 30%, 113% (partial) and 54%, 98% (complete) of the subcomponent total, for bCalf and bAdult respectively. (4) Osteoarthritic degeneration did not markedly affect Z^{OC} in adult human remnant tissue from surgeries. In 1x

PBS, Z^{OC} was indistinguishable between osteoarthritic total knee replacement tissue (OA-hAdult, 92 ± 37 %) and normal allograft tissue (NL-hAdult), with ScP accounting for 100% OA-hAdult and 99% of NL-hAdult. Z^{ScP+TB} in OA-hAdult was 106 ± 58% of NL-hAdult. Similar trends were evident after soak in 1/10x PBS.

These studies established the increasing contribution of ScP to Z^{OC} with maturation. Z^{OC} is a biophysical property that may have novel applications to biomimetic OC tissue engineering.

CHAPTER 1

INTRODUCTION

1.1 General Introduction To The Thesis

Articular cartilage (AC) is separated from trabecular bone (TB) by a thin region called the subchondral plate (ScP). These three components together form an osteochondral core (OC). Articular cartilage is composed of extracellular matrix (ECM), chondrocytes, water, collagen, and proteoglycans [35]. Trabecular bone underneath the articular cartilage is porous and has a lattice structure that is filled with bone marrow [6,32]. The subchondral plate which anchors the articular cartilage to the trabecular bone is composed of dense cortical bone and calcified cartilage(CC) [6, 9]. These components change with development and disease progression [9, 19]. Most notably, the subchondral plate thickens and increases in porosity with progression of osteoarthritis and becomes denser with maturation [9, 19, 37].

Due to the distinct properties of each tissue type (AC, ScP, TB) bioimpedance measurements can be performed in a conductive solution to characterize the structure of the tissue in various states. The proteoglycans, composed of molecules called glycosaminoglycans (GAGs), in articular cartilage contribute to the tissue having a high fixed charge density (FCD). The FCD of the tissue concentrates ions in solution preferentially in the cartilage and helps conduct current, creating a lower impedance than expected for the geometry of the sample [19, 30]. The lattice structure of trabecular bone is mainly filled with bone marrow, which is known to have a characteristic impedance, but can be removed by implementing centrifugation [3, 31, 32]. The cortical bone component of the ScP is known to have a characteristic resistivity that is much higher than that of trabecular bone[3, 9]. With the knowledge that the subchondral plate changes with maturation and degeneration, subchondral plate was predicted to be the main source of impedance

variation between different states (mature/immature, normal/osteoarthritic) of marrow-cleansed osteochondral tissue.

The overall motivation of this thesis was to determine if impedance of an osteochondral core varies with marrow removal of the trabecular bone, maturation or degeneration of the subchondral plate with osteoarthritis, and NaCl bath concentration. The main objectives of this work were to determine if the impedance: (1) of whole immature bovine osteochondral is reduced after centrifugation to remove bone marrow, (2) of bovine osteochondral cores and corresponding subchondral plate is increased by maturation, and (3) of human osteochondral cores and their corresponding subchondral plate are decreased by degeneration with osteoarthritis.

Chapter 1 starts with a brief background of articular cartilage, trabecular bone, and the subchondral plate which comprise an osteochondral core. This was followed by a discussion of how maturation and osteoarthritis affect these components structurally. Relevant properties of these tissues were detailed and how they contribute to overall electrical properties of tissue. This chapter also includes relevant calculations and design choices made in the execution of this project.

Chapter 2 describes the experimental design and execution of osteochondral core impedance. This included (1) calculating resistivity of PBS from impedance measurements, (2) investigation of marrow removal from immature bovine osteochondral cores and its effects on electrical impedance of a tissue sample, (3) investigating the effects of maturation on the impedance of a whole bovine osteochondral core and its individual subcomponents and (4) investigating the effects of osteoarthritis on the impedance of a whole human osteochondral core and its individual components. Resistivities of the subcomponents were computed for better comparison of the material properties of the different tissue types.

Chapter 3 of this paper summarizes the findings and possible future directions for similar work.

1.2. GLOSSARY OF TERMS

AC	Articular Cartilage
Ag/AgCl	Silver, Silver Chloride
bAdult	Mature bovine osteochondral core
bCalf	Immature bovine osteochondral core
bOC	Bovine Osteochondral Core, immature or mature tissue
C_i	Concentration of specific ion, i, in solution
CC	Calcified Cartilage
Cl^-	Chloride ion in solution
D^i	Diameter for arbitrary component, i
ECM	Extracellular matrix
FCD	Fixed Charge Density
GAG	Glycosaminoglycan
HA	Hydroxyapatite
ID^i	Inner diameter of corresponding reservoir system tube, i
OA	Osteoarthritis/Osteoarthritic
OA-hAdult	Osteoarthritic Human Osteochondral Core
OC	Osteochondral Core
PE	Polyethylene
hOC	Human Osteochondral Core
L^i	Length of a component of the tissue or reservoir system, i
Na^+	Sodium ion in solution
NL-hAdult	Normal Human Osteochondral Core

PBS	Phosphate-buffered saline; Buffer solution that maintains physiological conditions
ScBP	Subchondral Bone Plate; Cortical Bone component of the subchondral plate
ScP	Subchondral Plate; ScBP and Calcified cartilage together
TB	Trabecular bone
$\mathbf{V_i}$	Valence of an ion, i
$\mathbf{Z^i}$	Impedance from a particular component, i; Solution, polyethylene supports, osteochondral core, articular cartilage, or subchondral plate and trabecular bone
ρ^i	Resistivity of a parameter, i; Solution, Polyethylene supports, osteochondral core, articular cartilage, or subchondral plate and trabecular bone
μ_i	Ion electrical mobility constant of an ion, i; describes a specific ion's diffusion behavior

1.3 Articular Cartilage Structure And Function

In humans, articular cartilage is a 2-4 mm thick tissue layer located on the epiphysis of skeletal bones which serves to reduce load and friction in the joints [35]. It is composed of an extracellular matrix (ECM) with chondrocytes distributed throughout. The composition of ECM is mainly water (55-85%), collagen (10-20%), and proteoglycans (5%) which all contribute to load reduction on the tissue [35]. Proteoglycans are molecules composed of a protein core with many molecules called glycosaminoglycans (GAGs) bound covalently [35]. These molecules are important for the material properties of cartilage that contribute to lubrication of the joint and overall health of the cartilage [12].

Three distinct zones can be identified in articular cartilage: superficial, middle, and deep. The superficial zone is 10-20% of the total thickness, while the middle zone is 40-60% of the volume, and the deep zone is 30% of the volume. Each zone has unique properties due to the variations in composition. The superficial zone contains many chondrocytes and contributes to tensile properties of the tissue. The middle zone, the largest, contains proteoglycans and thick collagen fibrils which contribute to compressive load reduction. The deep zone has the highest proteoglycan content and largest collagen fibrils, providing the most mechanical resistance to compressive loads [35]. Below the deep zone of the articular cartilage is the calcified cartilage, which is distinguished by the tidemark [35].

Articular cartilage lacks blood vessels, lymphatic vessels, and nerves, which makes it difficult for the tissue to self-repair, leading to a variety of diseases that occur with age, including osteoarthritis [28, 35]. The avascularity of articular cartilage causes it to rely on the synovial fluid for nutrient diffusion [35].

1.4 Subchondral Plate Structure And Function

Separating the articular cartilage from the trabecular bone, is the subchondral plate (ScP). The subchondral plate is made of cortical bone, referred to as the subchondral bone plate (ScBP), and calcified cartilage (CC) [28, 38]. The typical thickness of the ScP is 216 ± 68 μm for females and 229 ± 52 μm for males [9]. This thin plate lies just below the articular cartilage, functioning as an anchor for the relatively soft articular cartilage onto the much more durable bone below as well as regulating cartilage metabolism [9, 28, 36].

The calcified cartilage lies just below the articular cartilage, separated by the tide mark, and above the ScBP, separated by the cement line [28]. This tissue has properties generally intermediate to those surrounding it and acts as a gradual transition from the soft unmineralized articular cartilage and the tough subchondral bone [28].

The ScBP is composed of dense, mineralized, cortical bone [6, 9]. The mass density of cortical bone is typically in the range of 1.6 -2.0 g/cm^3[16]. The dry weight of this tissue is ~80% hydroxyapatite (HA), leading cortical bone to be highly mineralized relative to trabecular bone [4]. In a healthy joint, the subchondral plate has low porosity to keep the articular cartilage mostly separate from underlying trabecular bone [9, 11]. Within the ScP there are vascular channels which supply the CC with nutrients [28].

The subchondral plate is known to be a critical component in the pathogenesis of osteochondral diseases, like osteoarthritis, and its degeneration can have lasting effects on the surrounding tissues [36].

1.5 Trabecular Bone Structure And Function

Trabecular bone, like articular cartilage, is found at the epiphysis of long bones and serves to distribute mechanical loads [32]. This bone has a lattice structure that is filled by soft bone marrow [32]. The trabecular bone is generally quite porous [6]. It is composed mainly of HA, collagen, and water, but is generally less mineralized than other bone types like cortical bone [32]. The tissue density of trabecular bone itself is 1.874×10^{-3} g/cm^3 [15].

The trabecular bone functions as a shock absorbing component for the osteochondral tissue, allowing dissipation of loads applied to the joint [36]. The hollow spaces in the trabecular bone are filled with bone marrow [32]. When the bone marrow is removed from the trabeculae, the tissue is largely hollow space.

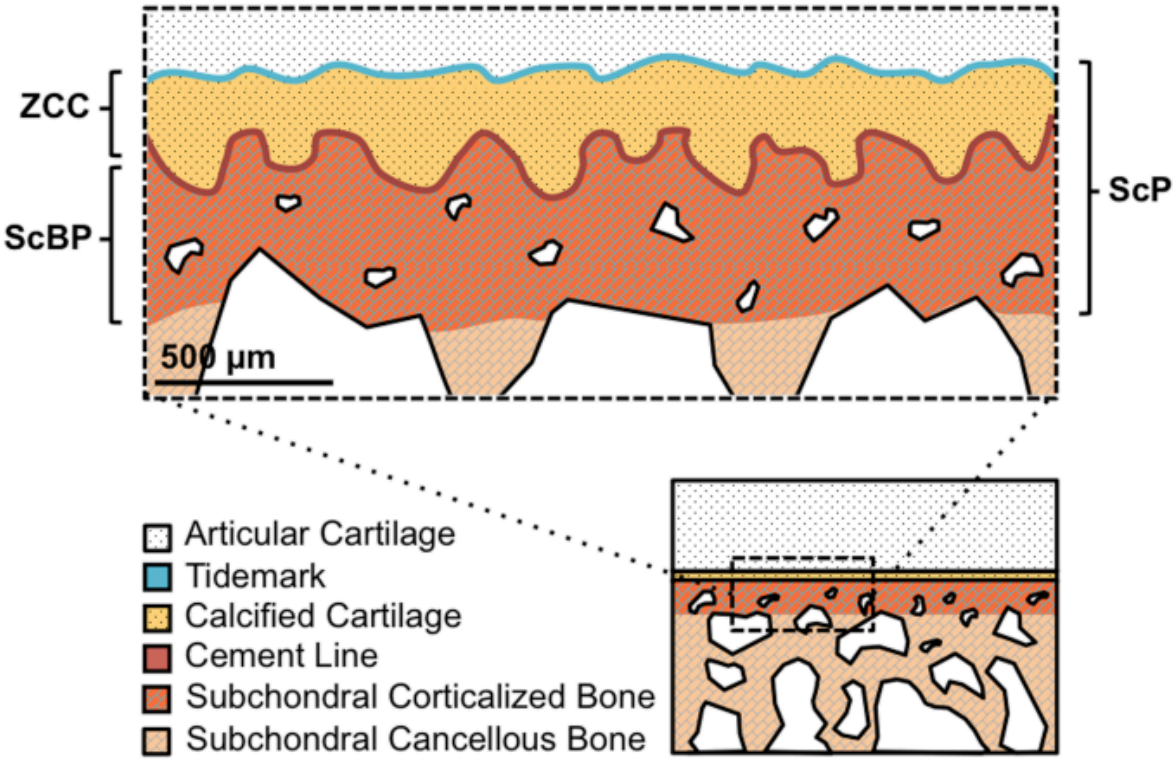

Figure 1.1: Schematic depicting the osteochondral interface, including the articular cartilage (AC), subchondral plate (ScP) composed of the subchondral bone plate (ScBP) and calcified cartilage (CC), and underlying trabecular (cancellous) bone (TB) [38].

1.6 Osteochondral Changes During Development

Immature AC is much thicker than that of mature tissue, as mechanical stresses from weight bearing have not yet caused thinning of the cartilage layer [19]. Cartilage calcification has been found to occur at the end stages of cartilage development, indicating that immature articular cartilage is less mineralized than mature cartilage [19]. Creeping mineralization at the interface between cartilage and trabecular bone causes the eventual shortening of the articular cartilage, which accounts for the variation in cartilage thickness with maturity [19]. In mature tissue, the highly mineralized component of the osteochondral core is smooth and distinct, whereas in the immature tissue the mineralized section is irregular and less developed[19]. The immature tissue shows higher levels of vascular invasion than when it is skeletally mature [20]. Vascular invasion connects the nutrient supply of the subchondral bone to the articular cartilage [19]. The mean thickness of mature bovine subchondral plate has been shown to be 869.5 ± 244.6 μm, whereas immature tissue had a mean thickness of 494.4 ± 135.4 μm [37]. Mature tissue was also shown to have a higher level of mineralization when compared to immature tissue throughout the entire subchondral region [37].

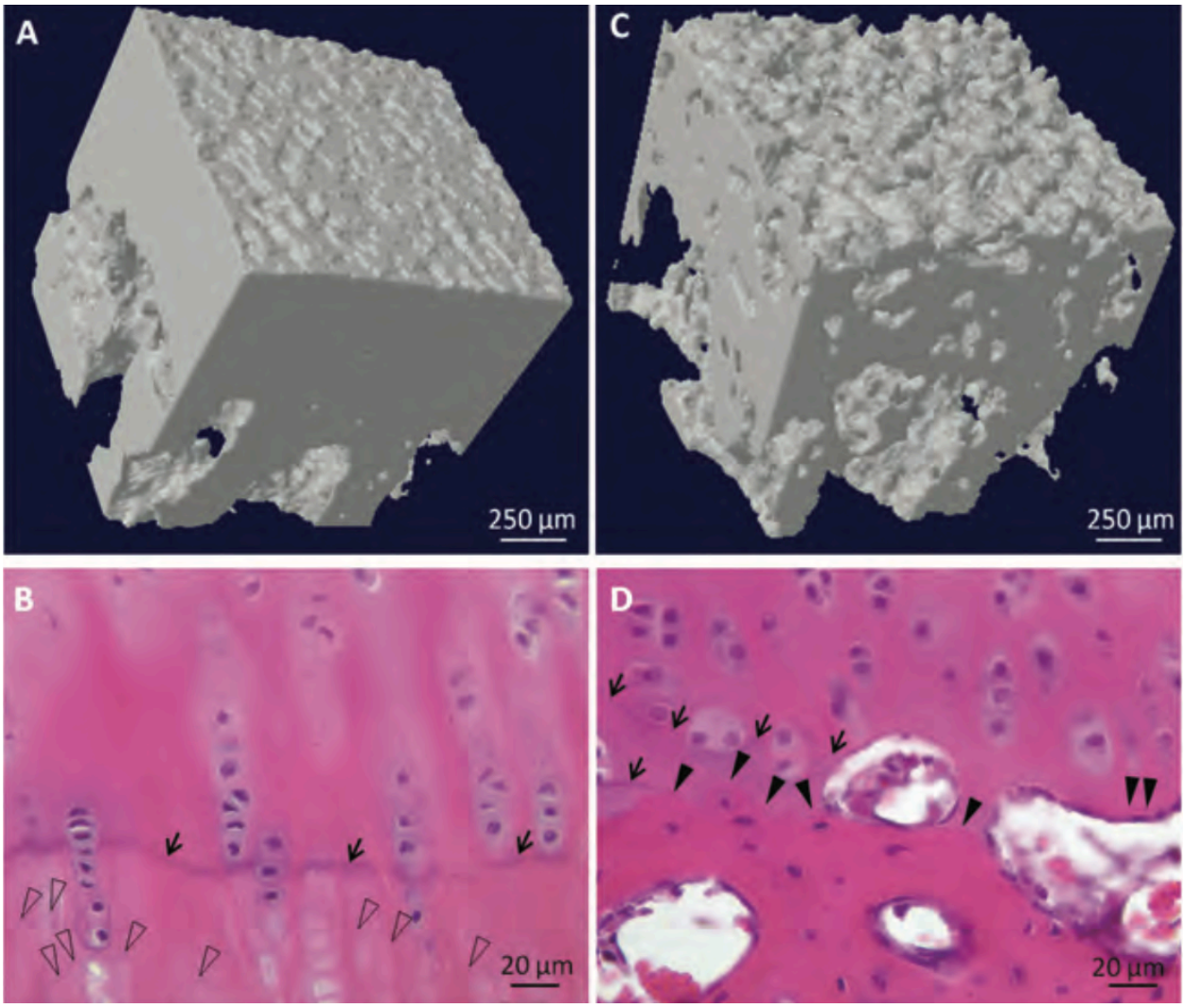

Figure 1.2: Changes to the osteochondral interface in a rabbit trochlea with normal skeletal maturation. (A, B) skeletally mature tissue (30 months), (C, D) skeletally immature (4 months). Panels A and C show 3D reconstructions from µCT scans. Panels B and D show Hematoxylin & eosin stain results of the tissues. The tidemark is shown by the small black arrows. Duplicating tidemarks are shown by open arrow heads. Solid black arrowheads demarcate the bone osteoid [19].

1.7 Osteochondral Changes During Progression Of Osteoarthritis

Osteoarthritis (OA) is a degenerative joint disease in which many biological factors play a role [7]. It is generally characterized by worsening cartilage deterioration and sclerosis of the subchondral bone [5, 25]. Recent studies have found increasing importance of the subchondral plate in the progression of osteoarthritis [36].

1.7.1 Causes of Osteoarthritis

Due to articular cartilage's avascularity, it is unable to heal itself upon incurring damage [35]. There are different factors that can contribute to damage and an individual developing osteoarthritis; however, the main risk factors include joint injury, genetic predisposition, obesity, and aging [7]. The molecular mechanisms at play are still poorly understood, and there is no effective therapeutic treatment for osteoarthritis [7].

1.7.2 Human Osteoarthritis Structural Changes

With the progression of OA, each of the three subcomponents of the OC detailed above undergo characteristic changes.

Changes to Trabecular Bone. In early osteoarthritis, the trabecular bone undergoes elevated remodeling and bone loss [27]. In later stages of OA, there is reduced mineralization to the bone as well as increased trabecular thickness and increased bone volume [7]. The bone also exhibits reduced mineralization and trabecular integrity [9].

Changes to the Subchondral Plate. With the onset of OA, the ScP can become thicker as well as becoming more porous [9, 24, 23]. This thickening is a result of the increased bone remodeling rate [6]. With the progression of OA, vascular channels that supply the tissue with nutrients also begin to invade the articular cartilage, creating new pathways for diffusion into articular cartilage that did not originally exist [6, 28]. Vascular channel invasion leads to increased

molecular crosstalk between the ScP and AC [39]. Studies have shown that the vascular channels in the ScP allow for increased fluid flow across the osteochondral interface with the progression of OA [21]. Other studies implementing Fluorescence Loss in Photobleaching (FLIP) techniques have also demonstrated higher diffusion across OA tissue due to the increased vascular invasion [39].

Changes to Articular Cartilage. The cells that exist in cartilage, chondrocytes, are typically quiescent. With the onset of OA, these cells undergo a shift in phenotype which results in surface fibrillation and matrix degradation [14]. Fissures in the cartilage emerge as the matrix proteoglycans break down, and the collagen erodes [13]. Notably, the progression of OA is directly related to proteoglycan loss which consequently reduces the hydraulic pressure of the tissue [33]. The collagen structure, which comprises the ECM, is altered leading to changes in mechanical properties of the tissue with disease progression [33]. The cartilage is also invaded by vascular channels of the ScP as previously described [14].

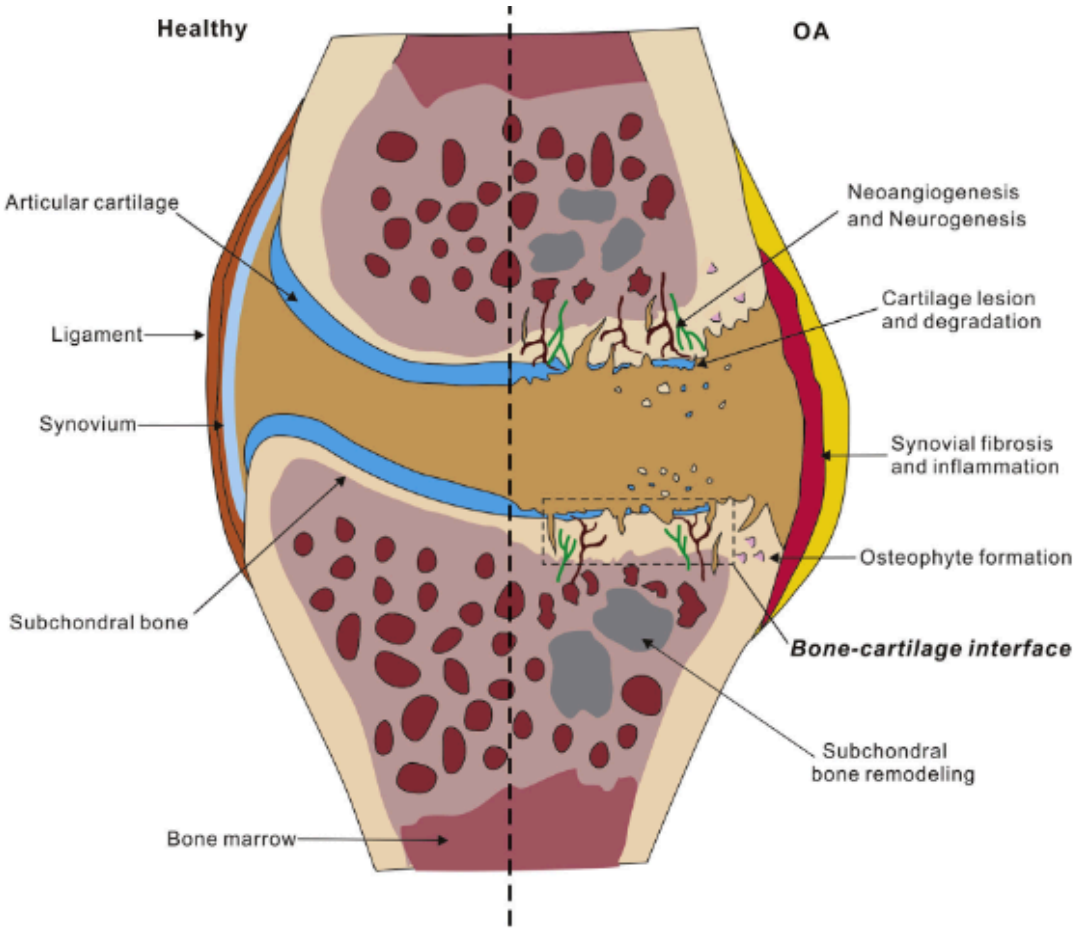

Figure 1.3: Schematic depicting relevant differences between a healthy joint and an osteoarthritic human joint [39].

1.8 THEORETICAL CALCULATIONS OF SOLUTION IMPEDANCE

To make impedance (Z) measurements across the length of the tissue samples, the tissue in this project was equilibrated in conductive solution. Phosphate buffered saline (PBS) was utilized for the purposes of this study. Cylindrical sample dimensions and salt concentration will affect the relative measured resistance of the sample. Equation (1) and the defined variables in Table 1.1 below show the relationship between dimensions, concentration, and ion properties for theoretical resistance. The measurement reservoir system, schematized simply below in Figures 1.4 and 1.5, will also add an intrinsic background impedance to the measurement. Using predetermined conditions, theoretical for the predictions for the resistance of the system were calculated using Equations 1 through 4. The relevant ions in PBS are sodium (Na^+) and chloride (Cl^-). Table 1.1 below details the dimensions of the reservoir system and other variables used for calculations

$$R = \frac{\rho L}{A} = \frac{L}{\sigma A} \tag{1-1}$$

$$\rho = \frac{1}{\sigma} \tag{1-2}$$

$$\sigma = F \sum_i c_i * \mu_i * |V_i| \tag{1-3}$$

$$A = \pi \left(\frac{D}{2}\right)^2 \tag{1-4}$$

Where:

F=Faraday's constant = 96,485 [C mol^{-1}]
ρ= resistivity [Ω m]
σ= conductance [$\Omega^{-1}m^{-1}$]
L= length of conductor (reservoir tube) [m]
A= cross sectional area of conductor (reservoir tube) [m]
D=diameter of reservoir tube [m]
c_i= concentration of ion, I [M]
i= ion species (Na^+, Cl^-)
μ_i= ion mobility of ion, i [m^2 V^{-1} s^{-1}]
V_i= valence of ion, i [-]

Figure 1.4 A shows how resistance changes relative to dimensions of the tissue sample. Throughout this thesis, the terms impedance and resistance will be used interchangeably because the impedance at the test frequencies (100 Hz, 1 kHz, or 10 kHz) is essentially a pure resistance. The equipment formally assesses impedance, but the measured phase shift at these frequencies is nearly zero so that the impedance value is essentially a pure resistance. The theoretical analysis is simplified without needing to assess energy storage (capacitance or inductance) contributions.

Figure 1.4 B schematizes the different components of the measurement system that contribute to tissue impedance. Z_e represents impedance from the electrodes into the solution used in measurement. Z_s represents impedance due to current spreading from the electrode into the solution, 1x or 1/10x PBS. Z_T represents impedance of the tube, with or without tissue. The dimensions and configuration of the reservoir set up also affect the background impedance, as shown later in Figure 2.1. By performing impedance measurements (Z) utilizing the same electrodes and reservoir set up with and without tissue, the difference between the tissue impedance and background solution impedance (without tissue) will be established. With the electrical material properties (resistivity or conductivity) of the solution and the length of the tissue sample, this difference in impedance allows determination of the electrical material properties of the tissue, as derived in Chapter 2.

Different configurations of the measurement system will affect the measured impedance. The reservoir system incorporates three concentric tubes designed to hold a tissue sample securely around its circumference. Tubes of different lengths were used to reduce background impedance by reducing the length L, but also to ensure complete containment of the sample within the tube by ensuring it was long enough (i.e., for the long bCalf sample). Table 1.2 shows the calculated impedance for different configurations of tubes for the implemented reservoir set up.

A

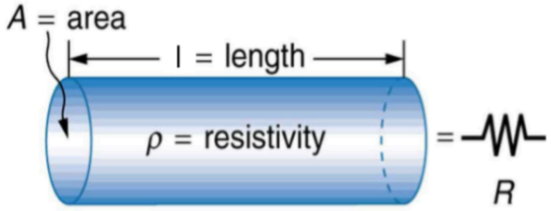

$$R = \frac{\rho L}{A} = \frac{1}{\sigma}\frac{L}{A}$$

Resistance of tube

B

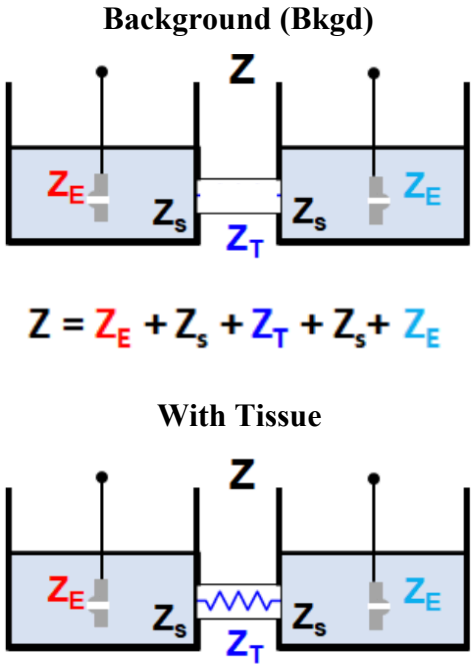

Figure 1.4: Contributions to resistance in a cylindrical sample and in a reservoir set up

Table 1.1: Dimensions of reservoir system 2.0 relevant for theoretical impedance, resistivity calculations

Variable	Definition	Value	Units
L^A	Tube A Length (short)	9.5	mm
	Tube A Length (long)	13.2	mm
ID^A	Tube A Inner Diameter	4.6	mm
L^C	Tube C Length	22.5	mm
ID^C	Tube C Inner Diameter	9.3	mm
F	Faraday's Constant	96,485	C/mol^1
C_{Na+}	Na^+ concentration (1x)	0.153 (1x)	Mol/L
	Na^+ concentration (1/10x)	0.015 (1/10x)	Mol/L
C_{Cl-}	Cl^- concentration (1x)	0.140(1x)	Mol/L
	Cl^- concentration (1/10x)	0.014 (1/10x)	Mol/L
μ_{Na+}	Na^+ Mobility	$5.19*10^{-8}$	$m^2 / (V^1 s^1)$
μ_{Cl-}	Cl^- Mobility	$7.91*10^{-8}$	$m^2 / (V^1 s^1)$
V_{Na+}	Na^+ Valence	1	-
V_{Cl-}	Cl^- Valence	-1	-

Table 1.2: Theoretical resistivity values for PBS (1x, 1/10x).

Solution	**Theoretical Resistivity [Ω·m]**
PBS (1x)	0.55
PBS (1/10x)	5.45

1.9 Electrical Properties Of Osteochondral Tissues

Electrical measurements have been used to characterize many types of biological tissues. Bone and fat provide relatively high resistance compared to the bathing solution [17]. Bioelectrical conductivity has a positive relationship with ion concentration and mobility [17]. The different tissue types that comprise an OC are thus predicted to each contribute to the electrical properties of the composite structure. By making impedance measurements on an OC and its individual subcomponents, these contributions can be assessed.

Articular Cartilage. Healthy AC is composed primarily of chondrocytes, and extracellular matrix, primarily collagen, proteoglycans, all of which are hydrated in a solution of water and dissolved solutes including ions [35]. The water component contributes negligibly to the electrical conductance of the tissue but contains the conductive ions [8]. Collagen is elastic, and piezoelectric behavior has been observed when the tissue is dry and dynamically stressed [2]. For the purposes of this project the articular cartilage will be hydrated and not undergo any dynamic stress, so that this contribution of collagen will be minimal. The primary cell type in cartilage, chondrocytes, are sparsely distributed throughout the ECM [35]. Due to their relatively low volume fraction relative to other components, chondrocytes are typically neglected when modelling tissue properties. The third component, proteoglycans, are rich in GAG molecules [35]. These molecules have a high density of deprotonated carboxylic acid and sulfate groups, which give the molecules a highly negative fixed charge density (FCD) [12]. FCD has been correlated to GAG content [30]. The immobile, negatively charged GAGs attract and increase the relative concentration of positively charged counter-ions in solution, leading to a Donnan potential across the cartilage interface [29]. This leads to a Donnan equilibrium, where the resultant total concentration of ions presents within the cartilage surface is greater than the concentration of ions in the solution [29]. These

concentrated ions affect the electrical properties of the cartilage— studies have shown that electrical conductivity of AC is dependent on FCD [18]. This is especially pronounced in solutions of low salt concentration, where the FCD and Donnan equilibrium maintains a relatively high electrical conductivity of articular cartilage. In general, overall tissue conductivity should increase with a high level of GAGs, as exists in healthy articular cartilage. Conversely, as AC degrades with OA, the conductivity of AC could decrease. As impedance is inversely related to conductivity, AC impedance (Z^{AC}) may be elevated with progression of OA.

Subchondral Plate. The subchondral plate is composed of dense cortical(-like) bone and calcified cartilage [6, 28]. Cortical bone has a resistivity on the order of kiloohm meters [3]. Thus, although thin, it may be the component of the OC contributing the highest series impedance. The ScP thickens with OA progression, which would cause an increase in electrical impedance with OA progression. However, the ScP also becomes vascular with OA progression allowing, water and solute flow and diffusion between the AC and the TB on either side of the plate [6, 9, 21]. The increased connectivity between the two ends of the OC could provide a pathway for current flow, more so than the cortical bone, and therefore may to lead to a decreased impedance with OA progression.

Trabecular Bone. The trabecular bone component of an OC has a characteristic resistivity; on the order of hundreds of ohm meters with marrow in place, much lower than that of cortical bone [3]. Due to its lattice structure, the bone itself is relatively sparse and it is mostly filled with bone marrow. Bone marrow is roughly 70% adipose tissue in human adults [10]. Because adipose tissue is mainly adipose and has little fluid or electrolytes, this tissue would contribute to the overall resistivity of the osteochondral core [10]. The bone marrow also works to prevent diffusion of any conductive solution deeper into the tissue for whole core impedance measurements [9]. In

order to minimize the effect of marrow on the assessment of impedance across the osteochondral interface, this marrow must be removed, which can be done via centrifugation [31].

1.10 REFERENCES

1. Amini M., Hisdal J., Kalvøy H., "Applications of bioimpedance measurement techniques in tissue engineering," JoEB, vol. 9, pp. 142-158, 2018.

2. Anderson J. C., Eriksson C., "Electrical properties of wet collagen," Nature, vol. 218, pp. 166–168, 1968

3. Balmer T. W., Vesztergom S., Broekmann P., Stahel A., Büchler P., "Characterization of the electrical conductivity of bone and its correlation to osseous structure," Sci Rep, vol. 8, p. 8601, 2018

4. Baumgartner R.N., Ross R. , Heymsfield S.B., "Does adipose tissue influence bioelectric impedance in obese men and women?," J Appl Physio, vol. 84, pp. 257–262, 1998

5. Bobinac D., Spanjol J., Zoricic S., Maric I., "Changes in articular cartilage and subchondral bone histomorphometry in osteoarthritic knee joints in humans," Bone, vol. 32, pp. 284–290, 2003

6. Burr D. B., Gallant M. A., "Bone remodelling in osteoarthritis," Nat Rev Rheumatol, vol. 8, pp. 665–673, 2012

7. Chen D., Shen J., Zhao W., Wang T., Han L., Hamilton J.L., Im H.J, "Osteoarthritis: toward a comprehensive understanding of pathological mechanism," Bone Res, vol. 5, p. 16044, 2017

8. Dean D.A., Ramanathan T., Machado D., Sundararajan R., "Electrical impedance spectroscopy study of biological tissues," J Electrostat, vol. 66, pp. 165–177, 2008

9. Fan X., Wu X., Crawford R., Xiao Y., Prasadam I., "Macro, micro, and molecular changes of the osteochondral interface in osteoarthritis development," Front Cell Dev Biol, vol. 9, 2021

10. Fazeli P. K., Horowitz M.C., MacDougald O.A., Scheller E.L., Rodeheffer M.S., Rosen C.J., Klibanski A., "Marrow fat and bone—new perspectives," J Clin Endocrinol Metab, vol. 98, pp. 935–945, 2013

11. Findlay D.M., Kuliwaba J.S., "Bone–cartilage crosstalk: a conversation for understanding osteoarthritis," Bone Res, vol. 4, pp. 1–12, 2016

12. Gandhi N. S., Mancera R.L., "The structure of glycosaminoglycans and their interactions with proteins," Chem Biol Drug Des, vol. 72, pp. 455–482, 2008

13. Goldring S.R., Goldring M.B., "Changes in the osteochondral unit during osteoarthritis: structure, function and cartilage–bone crosstalk," Nat Rev Rheumatol, vol. 12, pp. 632–644, 2016

14. Goldring M. B, “Articular cartilage degradation in osteoarthritis,” HSS Journal, vol. 8, pp. 7–9,. 2012

15. Gong J. K., Arnold J. S., Cohn S. H., “Composition of trabecular and cortical bone,” Anat. Rec., vol. 149, pp. 325–331, 1964

16. Grimal Q., Laugier P., “Quantitative ultrasound assessment of cortical bone properties beyond bone mineral density,” IRBM, vol. 40, pp. 16–24, 2019

17. Grimnes S., Martinsen Ø. G., “Bioimpedance and bioelectricity basics”, 3d edition. Cambridge, MA: Academic Press Inc., 2015

18. Hasegawa I., Kuriki S., Matsuno S., Matsumoto G., “Dependence of electrical conductivity on fixed charge density in articular cartilage,” Clin Orthop Relat Res, pp. 283–288, 1983

19. Hoemann C., Lafantaisie-Favreau C.-H., Lascau-Coman V., Chen G., Guzmán-Morales J., “The cartilage-bone interface,” J Knee Surg, vol. 25, pp. 085–098, 2012

20. Hunziker E. B., Kapfinger E., Geiss J., “The structural architecture of adult mammalian articular cartilage evolves by a synchronized process of tissue resorption and neoformation during postnatal development,” Osteoarthritis Cartilage , vol. 15, pp. 403–413, 2007

21. Hwang J., Bae W. C., Shieu W., Lewis C.W., Bugbee W.D., Sah R.L., “Increased Hydraulic Conductance of Human Articular Cartilage and Subchondral Bone Plate with Progression of Osteoarthritis,” Arthritis Rheum, vol. 58, pp. 3831–3842, 2008

22. Hwang J., “Integration of cartilage and bone through a calcified cartilage interface to form a functional osteochondral graft,” [PhD Thesis] UC San Diego, 2010

23. Iijima H., Aoyama T., Tajino J., Ito A., Nagai M., Yamaguchi S., Zhang X., Kiyan W., Kuroki H., “Subchondral plate porosity colocalizes with the point of mechanical load during ambulation in a rat knee model of post-traumatic osteoarthritis,” Osteoarthritis Cartilage , vol. 24, pp. 354–363, 2016

24. Intema F., Hazewinkel H.A.W., Gouwens D., Bijlsma J.W.J., Weinans H. , Lafeber F.P.J.G., Mastbergen S.C., “In early OA, thinning of the subchondral plate is directly related to cartilage damage: results from a canine ACLT-meniscectomy model,” Osteoarthritis Cartilage , vol. 18, pp. 691–698, 2010

25. Kamibayashi L., Wyss U. P., Cooke T.D.V., Zee B., “Trabecular microstructure in the medial condyle of the proximal tibia of patients with knee osteoarthritis,” Bone, vol. 17, pp. 27–35, 1995

26. Lesperance L. M., Gray M. L., Burstein D., “Determination of fixed charge density in cartilage using nuclear magnetic resonance,” J. Orthop. Res., vol. 10, pp. 1–13, 1992

27. Li G., Yin J. , Gao J. , Cheng T.S., Pavlos N.J., Zhang C., Zheng M.H., "Subchondral bone in osteoarthritis: insight into risk factors and microstructural changes," Arthritis Res Ther, vol. 15, pp. 1–12, 2013

28. Madry H., van Dijk C. N., Mueller-Gerbl M., "The basic science of the subchondral bone," Knee Surg Sports Traumatol Arthrosc, vol. 18, pp. 419–433, 2010

29. Maroudas A., "Physicochemical Properties of Cartilage in the Light of Ion Exchange Theory," Biophysical J, vol. 8, pp. 575–595, 1968

30. Maroudas A., Muir H., "The correlation of fixed negative charge with glycosaminoglycan content of human articular cartilage," Biochimica Biophys Acta Gen Subj, vol. 177, pp. 492–500, 1969

31. Naung N.Y., Suttapreyasri S., Kamolmatyakul S., Nuntanaranont T., "Comparative study of different centrifugation protocols for a density gradient separation media in isolation of osteoprogenitors from bone marrow aspirate," J Oral Biol Craniofac Res, vol. 4, pp. 160–168, 2014

32. Oftadeh R., Perez-Viloria M., Villa-Camacho J. C., Vaziri A., Nazarian A., "Biomechanics and mechanobiology of trabecular bone: a review," J Biomech Eng, vol. 137, pp. 0108021–01080215, 2015

33. Pearle A.D.,Warren R.F., Rodeo S.A., "Basic science of articular cartilage and osteoarthritis," Clin Sports Med, vol. 24, pp. 1–12, 2005

34. Schmidt, T.A., "Proteoglycan 4 metabolism and boundary lubrication of articular cartilage." [PhD Thesis] University of California, San Diego, 2006.

35. Sophia Fox A.J., Bedi A., Rodeo S.A., "The basic science of articular cartilage: structure, composition, and function," Sports Health, vol. 1, pp. 461–468, 2009

36. Stewart H. L., Kawcak C. E., "The importance of subchondral bone in the pathophysiology of osteoarthritis," Front Vet Sci, vol. 5, p. 178, 2018

37. Taheri S.,Winkler T. , Schenk L.S., Neuerburg C.,.Baumbach S.F, Zustin J., LehmannW., Schilling A.F, "Developmental transformation and reduction of connective cavities within the subchondral bone," Int J Mol Sci, vol. 20, p. 770, 2019

38. Unger, J., "Integration of articular cartilage and trabecular bone through the formation of a calcified interface" [Master's Thesis], University of California, San Diego, 2013

39. Yuan X.L., Meng H.Y., Wang Y.C., Peng J., Guo Q.Y., Wang A.Y, Lu S.B.,"Bone-cartilage interface crosstalk in osteoarthritis: potential pathways and future therapeutic strategies" Osteoarthritis Cartilage, vol. 22, pp. 1077–1089, 2014

CHAPTER 2

IMPEDANCE MEASUREMENTS OF OSTEOCHONDRAL TISSUE AND ITS SUBCOMPONENTS, MEASURED IN TWO ELECTRODE, TWO RESERVOIR SYSTEM

2.1 ABSTRACT

Introduction: The electrical impedance (Z) across a biological structure can be a sensitive indicator of its state, varying with maturation or disease. The osteochondral core (OC) is a layered structure, comprised of articular cartilage (AC), subchondral plate (ScP), and subjacent marrow-filled trabecular bone (TB), that varies markedly with skeletal maturation and osteoarthritis (OA). The marrow of TB includes abundant fat which is relatively insulating. The ScP is absent in the immature epiphysis and forms during maturation. In adult humans, the ScP thickens and develops vascular channels with OA. The objectives of this study were to evaluate the effects of marrow removal, and maturation or degeneration of the subchondral plate on the electrical impedance across an OC (Z^{OC}), and to establish resistivity and conductivity values for selected subcomponents.

Methods: Electrical impedance measurements were made between pairs of silver/silver-chloride electrodes, each immersed in a reservoir that was separated from the other reservoir by a tube containing the bath solution or various samples. Samples consisted of osteochondral cores (OCs) harvested from the knees of calf (bCalf) and adult (bAdult) bovines, human allograft donors (NL-hAdult), human OA surgery patients (OA-hAdult). Bath solutions consisted of 1x PBS and 1/10x PBS. Solution and tissue resistivity values were calculated based on the relationship between resistance and cylindrical tube or tissue dimensions. (Exp 1) The resistivity values of 1x and 1/10x PBS solutions were assessed by measuring impedance at across tubes of varying lengths between two reservoirs. (Exp 2) The effect of marrow removal was assessed by measuring impedance

before and after centrifugation of immature bovine calf (bCalf) OC. (Exp 3) The effect of maturation was assessed by comparing impedance of bCalf and mature bovine (bAdult) OCs, and the contribution of subcomponents (AC, ScP+TB) was assessed by additional impedance measures of the separated portions. (Exp 4) The effect of human disease was assessed by analyzing normal (NL-hAdult) and osteoarthritic (OA-hAdult) OCs and their individual subcomponents (AC, ScP+TB).

Results: (Exp 1) The resistivity of PBS was 0.570 ± 0.002 Ω·m and 4.99 ± 0.08 Ω·m for 1x and 1/10x, respectively. (Exp 2) bCalf-Z^{OC} were reduced by 30% with marrow removal, with an effective marrow resistivity of 1.15 ± 0.15 Ω·m. (Exp 3) bCalf-Z^{OC} was 8% of bAdultZ^{OC}. bCalf- Z^{ScP+TB} was 5% of bAdult Z^{ScP+TB}. The resistivity of bAdult OC was 1.71 ± 0.33 Ω·m while bCalf was 0.90 ± 0.15 Ω·m. The resistivity of bAdult ScP+TB was 11.00 ± 4.86 Ω·m and bCalf ScP+TB was 1.27 ± 0.13 Ω·m. (Exp 4) OA-hAdult-Z^{OC} was 84% of NL-hAdult-Z^{OC}. OA-hAdult-Z^{ScP+TB} was 92% of NL-hAdult-Z^{ScP+TB}. The subchondral plate was the main source of impedance for whole OCs. Resistivity of the NL-hAdult-OC was 8.98 ± 2.77 Ω·m, while OA-hAdult-OC was 4.98 ± 1.06 Ω·m. Resistivity of the ScP+TB was 10.50 ± 3.86 Ω·m and OA-hAdult was 8.14 ± 2.41 Ω·m.

Discussion: Experiments (1) and (2), established methods or assessing the impedance across OCs. (3) Followed expectations with established changes to tissue for marrow removal and maturation of the subchondral plate. Mature bovine subchondral plate resistivity values were in line with other studies Experiment (4) found there was no marked difference between NL-hAdult and OA-hAdult tissue, though both had the ScP+TB as the overall source of impedance and resistivity.

2.2 INTRODUCTION

Structure and Composition of Osteochondral Core. Osteochondral cores are composed of three subcomponents of distinct tissue: articular cartilage (AC), subchondral plate (ScP), and trabecular bone (TB). Each of these subcomponents contribute distinctly to the overall properties of the core. Trabecular bone has a lattice structure which is filled with bone marrow [17]. Bone marrow is 70% fat and fills what would otherwise be negative space in the trabecular bone [3]. The articular cartilage is composed of an extracellular matrix (ECM) with chondrocytes sparsely distributed throughout [19]. The composition of ECM is mainly water (55-80%), collagen (10-20%), and proteoglycans (5%) [19]. Proteoglycans are molecules composed of a protein core with many molecules called glycosaminoglycans (GAGs) bound covalently [19]. The subchondral plate (ScP), which separates the AC from the TB, is composed of dense cortical bone and the calcified cartilage [2, 4, 14].

Maturation. The articular cartilage for immature tissue is much thicker than that of mature tissue [9]. There is also more vascular invasion in immature tissue connecting the subchondral bone to the articular cartilage [9]. In bovine tissue, the subchondral plate increases in density and mineralization with maturity as well as becoming more well defined [9, 19].

Osteoarthritis Progression. As osteochondral tissue develops osteoarthritis, the articular cartilage's proteoglycans begin to break down [6]. The AC is also invaded by vascular channels, leading to higher crosstalk with the subchondral bone [20]. These same vascular channels increase the porosity of the subchondral plate, leading to increased ability for fluid to flow across the OC [10 , 4]. The subchondral plate also increases in thickness with the progression of osteoarthritis and the tidemark, the mineralized component which separates the CC from the AC, can multiply leading to increased presence of mineralized tissue [2].

Impedance Measurements. Tissues can be characterized using bioimpedance measurements [1]. For the purposes of this study, the structure of an osteochondral core can be characterized with electrical impedance measurements of the whole sample and its individual components. Figure 2.1 schematizes the different configurations of impedance measurements made in the execution of this study.

Electrical Properties of Osteochondral Tissues. Trabecular bone and bone marrow have an established resistivity [1]. In order to reduce the effects of trabecular bone on overall core impedance, bone marrow can be removed via centrifugation [15].The relatively porous trabecular bone would not greatly contribute to the core's impedance after the bone marrow has been removed and replaced with conductive solution. The main components of articular cartilage are also not expected to greatly contribute to core impedance. The main components (water, chondrocytes, and collagen) would be overridden by the effects of proteoglycans and their glycosaminoglycans (GAGs). These molecules have many deprotonated carboxylic acid and sulfate groups, which give the molecules a highly negative fixed charge density (FCD) [5]. FCD has been correlated to GAG content [15]. The presence of a FCD attracts ions present in solution to be concentrated closer to the surface of the tissue, in what is called a Donnan Equilibrium. Other studies have shown that electrical conductivity of AC is dependent on FCD, meaning GAG content has a positive relationship with electrical conductivity of cartilage tissue [9].Overall tissue conductivity should increase with a high level of GAGs, as exists in healthy articular cartilage, therefore the articular cartilage is not expected to add to impedance of an osteochondral core. The remaining component of the osteochondral core, the subchondral plate, has a cortical bone component which is known characteristic resistivity higher than that of trabecular bone, on the order of kiloohm meters as

opposed to hundreds of ohm meters [1]. This characteristic resistivity of the cortical bone would cause the subchondral plate to be the main source of overall core impedance.

The objectives of this study were to evaluate the variation in electrical impedance across OCs with normal maturation and osteoarthritic degeneration. To establish the measurement system, (1) the impedance of 1x and 1/10x PBS bath solutions was determined, and (2) the effect on OC impedance of centrifugal removal of marrow was assessed. Then, the effect on OC impedance of (3) bovine maturation and (4) human OA, as were effects on the AC and ScP+TB components.

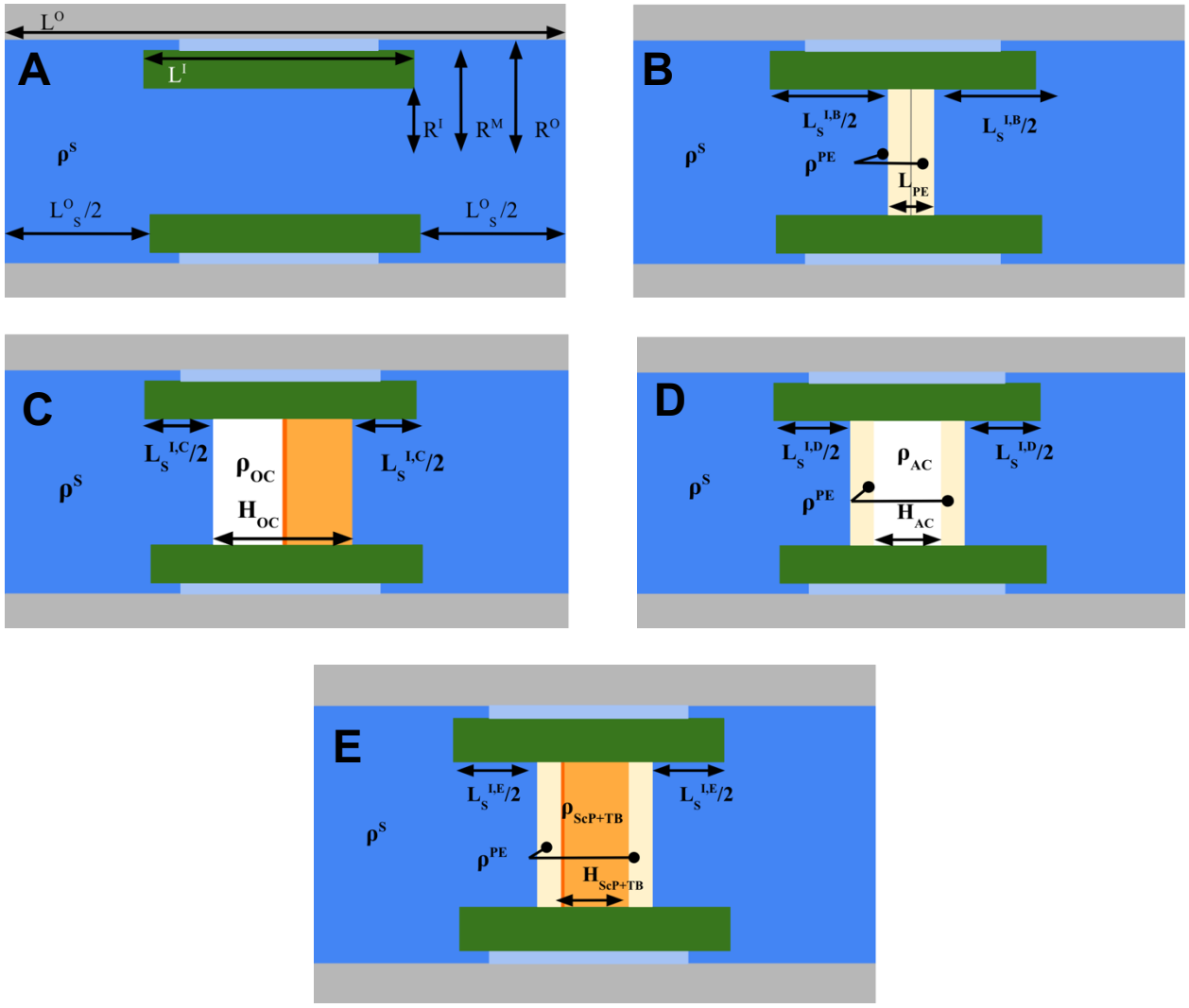

Figure 2.1: Schematic of the reservoir system implemented for impedance measurements. Panel (A) shows the reservoir tubes filled with PBS. Panel (B) shows the porous polyethylene supports implemented to keep thin tissue segments in place. Panel (C) shows the tubes containing a whole, arbitrary OC. Panel (D) shows the articular cartilage held in place by PE supports. Panel € shows the subchondral plate and trabecular bone section held in place with PE supports. Each configuration has relevant resistivities labelled.

2.3 Equation Derivations For Reservoir Configurations

From the measured impedance Z of each reservoir configuration detailed in Figure 2.1, an equation for the material property resistivity, ρ, can be derived for each component. Each component of the configuration contributes its own specific impedance to the overall measured impedance. The individual contributions can be added together to represent the entire impedance. With some rearrangement, the equation for impedance can be converted into an equation for the material property resistivity, ρ.

Configuration A in Figure 2.1 shows the configuration for basic background measurements performed, with the reservoir system filled with PBS. The impedance measurement made in this configuration, Z^A, can be represented by the following equation:

$$Z^A=\rho^S\cdot[L_S^O/ (\pi \cdot(R^O)^2) + L^I/(\pi\cdot(R^I)^2)] \quad (2\text{-}1)$$

From this equation, the resistivity of the solution, ρ^S, can be derived by rearranging the equation algebraically.

$$\rho^S= Z^A/ [L_S^O/(\pi\cdot(R^O)^2) + L^I/(\pi\cdot(R^I)^2)] \quad (2\text{-}2)$$

Similarly, the configuration detailed in Figure 2.1 B shows the configuration for background impedance utilizing polyethylene (PE) supports. The thin articular cartilage post-sectioning needed to be supported in the reservoir system to ensure proper measurement. For this, the PE supports were used, and any additional impedance was accounted for as background impedance for the measurement configuration. The impedance of this configuration, Z^B, can be written as:

$$Z^B =\rho^S[L_S^O/(\pi\cdot(R^O)^2) + L^{I,B}/(\pi\cdot(R^I)^2)] +\rho^{PE}(L_{PE}/(\pi\cdot(R^I)^2) \quad (2\text{-}3)$$

This can then have the PBS background subtracted (Z^A) to give impedance of just the polyethylene supports. Then, the whole equation can be rearranged to determine resistivity of the polyethylene support, ρ^{PE}.

$$\rho^{PE} = \rho^S + (Z^B - Z^A)\cdot((\pi\cdot(R^I)^2) / L_{PE}) \quad (2\text{-}4)$$

Panels C-E show the various tissue configurations in the reservoir system. Panel C shows the whole intact OC prior to sectioning. The impedance of this configuration can be written as:

$$Z^C = Z_S{}^C + Z_{OC} = \rho^S[L_S{}^O/(\pi\cdot(R^O)^2) + L^{I,C}/(\pi\cdot(R^I)^2)] + \rho_{OC}[H_{OC}/(\pi\cdot(R^I)^2)]$$

Impedance measurements made in this configuration had the background removed by subtracting measurements made in configuration A—the reservoir system with just PBS. This adjustment for background impedance can be represented with the following equation:

$$Z^C - Z^A = \rho^S\,[L^{I,C}/(\pi\cdot(R^I)^2) - L^I/(\pi\cdot(R^I)^2)] + \rho_{OC}[H_{OC}/(\pi\cdot(R^I)^2)] \quad (2\text{-}5)$$

This can be simplified by converting the $L^{I,C}$ and L^I terms into $-H_{OC}$ and grouping terms by resistivity term.

$$Z^C - Z^A = \rho^S \cdot [-H_{OC}/(\pi\cdot(R^I)^2)] + \rho_{OC}[H_{OC}/(\pi\cdot(R^I)^2)] \quad (2\text{-}6)$$

Simplifying further, the resistivities can be group together.

$$Z^C - Z^A = (\rho_{OC} - \rho^S) \cdot [H_{OC}/(\pi\cdot(R^I)^2)] \quad (2\text{-}7)$$

From this, a final equation for resistivity of the whole OC can be determined.

$$\rho_{OC} = \rho^S + (Z^C - Z^A)\cdot((\pi\cdot(R^I)^2) / H_{OC}) \quad (2\text{-}8)$$

A similar derivation can be implemented for configurations D and E, subtracting out background impedance from configuration B with the PE supports, Z^B. For the articular cartilage (D) and subchondral plate and trabecular bone (E) measurements, the total impedance can be written as:

$$Z^D = Z_S{}^D + Z_{AC} + 2\cdot Z^{PE} \quad (2\text{-}9)$$

$$Z^E = Z_S^E + Z_{ScP+TB} + 2 \cdot Z^{PE} \quad (2\text{-}10)$$

A similar derivation process can be followed to obtain resistivity of the AC, ρ_{AC}, and ScP+TB, ρ_{ScP+TB}, resulting in the following equations:

$$\rho_{AC} = (Z^D - Z^B) \cdot ((\pi \cdot (R^I)^2)/H_{AC}) \quad (2\text{-}11)$$

$$\rho_{ScP+TB} = (Z^E - Z^B) \cdot ((\pi \cdot (R^I)^2)/H_{ScP+TB}) \quad (2\text{-}12)$$

With each of these derived equations, resistivity values can be calculated for each component of the system based on impedance measurements.

2.4 MATERIALS AND METHODS

Experimental Design. (1) The resistivity of PBS 1x and 1/10x were established for background contribution of measurement solution to overall resistivity. Following this, the effects of (2) marrow removal from the trabecular bone, as well as (3) maturation (4) and degeneration of the subchondral plate on the impedance of an osteochondral core were assessed. Osteochondral cores (OCs) (d=4.9mm) composed of trabecular bone (TB), a subchondral plate (ScP), and articular cartilage (AC) were harvested from the femoral condyles of human and bovine knee joints. Samples were prepared for consistency prior to impedance measurements being performed.

Experiment 1 used tubes of different lengths and three sets of paired electrodes to experimentally determine ρ^{PBS} for 1x and 1/10x PBS. Linear regression was performed to determine slope and intercept of the impedance vs tube length for each electrode pair. Using the geometry, equation 1-1 ($R = \frac{\rho L}{A}$), and slope, the resistivity was estimated for each electrode pair. Slope, intercept, and resistivity values were described as mean ± SD.

Experiment (2) used immature (1-3 weeks old) bOCs (n=9) that underwent impedance measurements before and after marrow removal via centrifugation. Measurements for each treatment group of osteochondral cores were averaged together and plotted in clustered bar charts to compare between pre- and post- marrow removal. For each configuration, the measured background impedance was subtracted from each measurement to better illustrate the differences between only the tissue samples. This is shown as Δ impedance. To compare samples before and after marrow removal, a two-tailed paired t-test was performed. Measured impedance changes (Δ Ω) were plotted against removed pellet mass (g) and a linear regression analysis was performed to assess the relationship between impedance drop and marrow loss. Using an approximation for density (0.89 g/cm^3) of bone marrow, a volume was estimated for the removed marrow [7].

Assuming the marrow volume to be a cylindrical disc within the tube the apparent resistivity (ρ^{Marrow}) was computed using marrow and sample length, Equation 1-1, and the drop in impedance associated with the loss of marrow.

Experiments (3, 4) used bovine (bCalf and bAdult) and human (NL-hAdult and OA-hAdult) samples (n=9 for each group), which underwent impedance measurements in PBS for whole OC and individual subcomponents. Impedance measurements between groups were compared to understand the effects of (3) maturation of the subchondral plate and (4) degeneration of the subchondral plate with OA progression. Measurements in experiments 3, 4 were corrected for background impedance based on the configuration in which measurement was performed (i.e., with or without PE supports). This data was shown as Δ impedance. Whole OCs initially underwent equilibration and impedance measurement in PBS 1x, followed by individual subcomponent measurements. To understand the effects of bath concentration on impedance measurements, equilibration and tissue subcomponent measurements were repeated in PBS 1/10x. Initially this was performed by allowing samples to sit in ~2ml PBS 1/10x on a nutator for multiple days. Additional desorption analysis was performed later in which bCalf (n=9) and bAdult (n=2) were again equilibrated at 4ºC on a nutator 1/10x solution, with a total volume of 50ml and underwent repeated impedance measurement. Results were compared between groups to determine if a significant difference in impedance was observed based on maturation or degradation. To compare samples of different tissue groups a repeated measures 2-way ANOVA was performed, followed by a t-test ($p<0.05$). Statistically significant data was marked with an asterisk (*) in the resulting figures. Impedance values were converted to estimates of resistivity ρ for the whole OC, AC, ScP+TB, as well as the polyethylene supports. The experimentally

determined ρ^{PBS} from experiment (1) was used for these calculations, as it agreed well with theoretically predicted ρ^{PBS} values.

Sample Harvest. Osteochondral cores were harvested from the femoral condyles of normal (allograft unused waste) human, osteoarthritis (total knee replacement waste) human, adult (1–3-year-old) bovine, and calf (1–3-week-old) bovine. For studies using human tissue, harvest was performed as previously described [17]. Briefly, osteochondral cores (4.9 mm diameter) were harvested from the femoral condyles of cadaveric tissue bank donors and discarded knee fragments from knee replacement surgery patients with Institutional Review Board approval. Three cores (n=3) were taken from each source (m=3) for both normal and OA tissue types using the Osteochondral Autograft Transfer System (Arthrex, Naples, FL). For studies using bovine tissue, harvest was performed as previously described [11]. In short, knees from 1–3-week-old and 1–3-year-old bovines with intact joint capsules were obtained from abattoirs. OCs (4.9 mm diameter) were harvested from the femoral condyles of the immature joints using the Osteochondral Autograft Transfer System (Arthrex, Naples, FL). Mature bovine osteochondral cores were harvested similarly using a drill press. Tissue was kept hydrated throughout harvest with PBS. Harvested cores were stored in PBS at 4ºC until further processing.

Table 2.1: Human tissue information.

Sample ID	Condition	Sex	Age [years]
NL-hAdult-1	Normal	M	44
NL-hAdult-2	Normal	F	22
NL-hAdult-3	Normal	F	24
OA-hAdult-1	Osteoarthritic	F	84
OA-hAdult-2	Osteoarthritic	F	60
OA-hAdult-3	Osteoarthritic	F	69

Sample Preparation. In order to standardize the interface and subchondral bone thickness of samples, excess trabecular bone was removed using a reciprocating saw (Cordless Driver 4100, Stryker, Kalamazoo, MI) to reduce bone size to ~2mm relative to the subchondral plate. When cores were ready for marrow removal, they were blotted dry, fit snugly into Tube A of the reservoir system (ID 4.76mm; OD 7.49mm; L 10.5-13.3mm; Silicone Rubber 35A durometer, McMaster-Carr, Elmhurst, IL), and placed in a microcentrifuge tube. Samples were centrifuged to remove bone marrow for 300s at 10,000g in Centrifuge 5324 (Eppendorf, Hamburg, Germany). Bubbles were removed from each core by applying negative pressure before equilibrating in a PBS filled container on a nutator overnight at 4ºC. When the applicable cores were ready for sectioning, the core was held securely in a clamp and the articular cartilage was cut horizontally using a scalpel.

Impedance Measurements. When cores were ready for impedance measurements, Tube A containing the core, or individual subcomponent, was placed in the reservoir system. The reservoir system was designed in such a way that it holds osteochondral cores (d=4.9mm) snugly around the circumference along the length of the core. Tube A (ID 4.76mm; Silicone Rubber 35A durometer, McMaster-Carr, Elmhurst, IL) is elastic to adjust to slight variations in core diameters. Tube B wraps around Tube A to ensure a snug fit upon insertion into Tube C, which connects to reservoirs on either end. For measurements made in reservoir configuration B, using PE supports, the discs were placed on either side of the tissue and firm pressure was applied with a blunt probe to ensure sample was upright and snug against supports. For measurements, both reservoirs were filled with PBS and the system was agitated to remove any bubbles from the connecting tubes. Measurements were made with an LCR (LCR Meter 879B, B&K Precision, Yorba Linda, CA) connected to flat, circular Ag/AgCl electrodes (Techonmed Engineering B.V., Maastricht,

Netherlands) via mini grabbers. Electrodes were placed at the opening of the connecting tube (Tube C) and impedance measurements were recorded after two seconds, after which time values had stabilized. Measurements were repeated across a range of frequencies: 100Hz, 1kHz, and10kHz. Background measurements were made for each reservoir system configuration with the respective solution in which measurements were made, either with or without PE supports depending on the relative length of the tissue.

2.5 RESULTS

Impedance Variation with Tube Length to Determine Solution Resistivity. Impedance increased linearly with tube length for both 1x and 1/10x PBS. Representative results for linear regression of one set of electrodes yielded $R^2 = 0.992, 0.997$ for 1x and 1/10x PBS, respectively. Overall, slopes (representing ρ/A) were 72.0 ± 0.2 Ω / mm and 631 ± 10 Ω / mm for PBS 1x and 1/10x respectively. Intercepts were 6.97 ± 0.24 Ω / mm (PBS 1x) and 38.4 ± 5.9 Ω / mm (PBS 1/10x) at 1kHz. Accounting for tube geometry the slopes yielded resistivity estimates 0.570 ± 0.002 Ω·m and 4.99 ± 0.08 Ω·m for PBS 1x and 1/10x, respectively.

Impedance Before and After Marrow Removal. The impedance of immature bovine tissue (bCalf) was decreased with marrow removal across all three measured frequencies. There was an average change of -60 Ω, or -30%. The paired t-test showed the decrease was significant with $P < 0.001$ for all frequencies.

Marrow removal was visually evident when comparing trabecular bone of OCs before and after centrifugation (Figure 2.3 A, B). Removed marrow was collected in the form of a pellet for each OC and the pellet mass was plotted against the individual change in impedance (Figure 2.3 D). The linear regression between change in impedance (Ω) and pellet mass (g) yielded $y = 3{,}566x - 38$ with $R^2 = 0.48$ ($p<0.05$).

Using geometry of the sample, the drop in impedance, and literature values for density of bone marrow, estimates for marrow resistivity were calculated. ρ^{Marrow} was calculated to be 1.15 ± 0.15 Ω m.

Table 2.2: Dimensions of osteochondral cores by subcomponent. Data is presented as mean ± SD.

Tissue Type	Length [mm]	D^{AC} [mm]	D^{ScP} [mm]	D^{TB} [mm]
bCalf	8.35 ± 1.53	4.64 ± 0.10	4.69 ± 0.19	4.66 ± 0.08
bAdult	3.88 ±0.71	4.80 ± 0.29	4.64 ± 0.20	4.63 ± 0.05
OA-hAdult	5.86 ± 0.54	4.91 ± 0.28	5.04 ± 0.20	4.97 ± 0.19
NL-hAdult	4.64 ± 0.55	4.95 ± 0.23	5.03 ± 0.19	4.91 ± 0.25

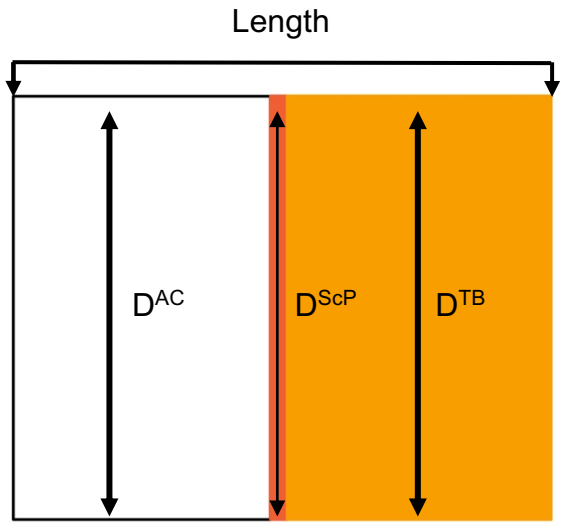

Figure 2.2: Schematic of dimensions of arbitrary osteochondral core; White zone represents the articular cartilage, the dark orange represents the subchondral plate, and the light orange represents the trabecular bone region.

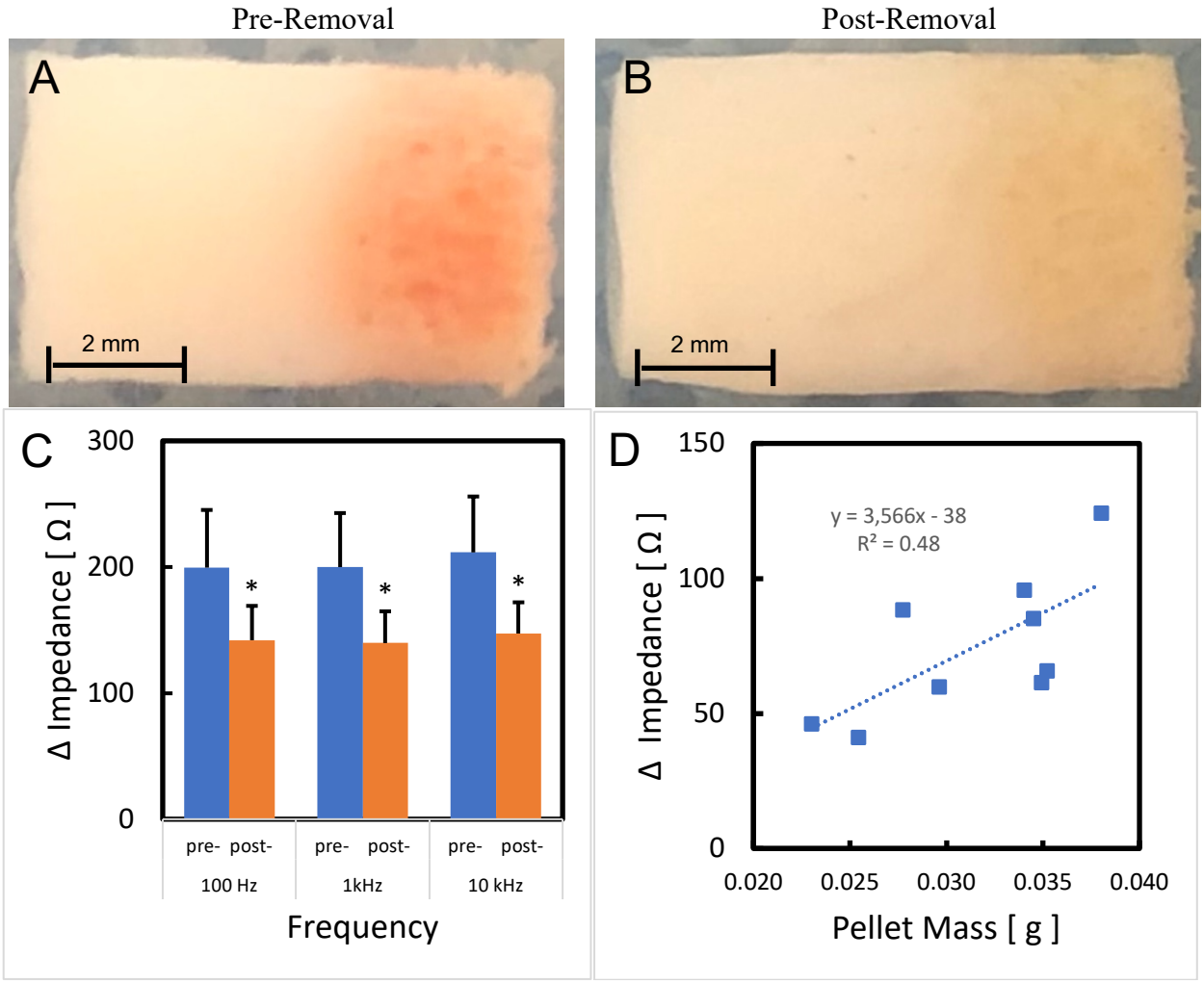

Figure 2.3: Effect of centrifugation for marrow removal on impedance across immature bovine osteochondral cores. (A, B) gross images of bCalf OC pre- and post- centrifugation (C) Impedance of samples in PBS 1x was adjusted for background (Δ impedance). Data are shown as mean ± SD, n=9. * Indicates $p<0.05$ by paired t-test. (D) Relationship between impedance at 1kHz and marrow released by linear regression.

Impedance of Immature and Mature Bovine Osteochondral Cores. Figure 2.4 shows representative images for each tissue type, bAdult and bCalf. The articular cartilage of the bCalf was consistently longer than that of the adult tissue, as expected. Gross images (A-D) illustrated the expected differences in tissue types, including the clearly visible separation between the AC and TB in bAdult tissue, and a more gradual transition between the two tissue types in bCalf tissue. μCT imaging confirmed the differences in subchondral plate structure between the two tissue types. The bony portions of the OCs are shown in white, and the AC appears black. For bAdult tissue, the subchondral plate is denser and more clearly defined, which can be seen by the brighter white at the interface of μCT images. The subchondral plate for bCalf tissue is undeveloped and there is a gradual transition from the AC in black, to the trabecular bone shown in white.

Table 2.3 shows the summary data collected for impedance measurements performed at 1kHz in PBS 1x—both raw data (A) and data corrected for background impedance from the reservoir system (B) are shown. Figure 2.5 (A, C) shows the whole core and subcomponent impedances, measured in PBS 1x at 1kHz, corrected for measured background impedance. For all measured frequencies—a difference was found between bAdult-Z^{OC} and bCalf-Z^{OC} ($p<0.001$). bCalf-Z^{OC} was 8% of bAdult-Z^{OC}. After tissue sectioning, it was found that the main source of the osteochondral core's impedance was due to the subchondral plate component—bCalf-Z^{ScP+TB} was 5% of bAdult-Z^{ScP+TB}. There was variation between measurements within the same group, with the highest variation occurring in the subchondral plate, and the lowest variation in the articular cartilage. The bAdult-Z^{AC} had an average impedance less than that of the background, whereas the bCalf-Z^{AC} samples had an average impedance slightly greater than the background measurements.

Table 2.3 shows the raw and adjusted summary data for impedance measurements made in low concentration PBS (1/10x). With a much lower salt ion concentration, the corrected impedance

for Z^{ScP+TB} was higher than that of the PBS 1x. Figure 2.5 (B, D) illustrate this data. For initial (2ml) soak, the bCalf-Z^{AC} was consistently lower than that of the background across all frequencies. The bAdult- Z^{AC} also was consistently lower than PBS, but of less magnitude than the bCalf tissue. For ScP components, the bAdult- Z^{ScP+TB} maintained the high impedance even in low salt concentrations. The bCalf-Z^{ScP+TB}, however, had an impedance slightly below the background. This is likely due to some components of the articular cartilage remaining attached to the ScP after sectioning, allowing a reduction in impedance. The bCalf-Z^{ScP+TB} was less in magnitude than the bCalf-Z^{AC} measurements, likely reduced by the ScP components of the tissue. Z^{ScP+TB} was 30% (bCalf) and 113% (bAdult) of the subcomponent total.

After equilibration in a larger volume of 1/10x PBS desorption analysis was performed on bovine samples to investigate the changes to impedance measurements after equilibration in a larger volume of 1/10x PBS. All average impedance values were now slightly greater than background measurements. Z^{ScP+TB} was 54% (bCalf) and 98% (bAdult) of the subcomponent total.

Resistivity values were calculated for each configuration utilizing derived equations detailed in section 2.3 above. Results are summarized in Table 2.4. ρ^{PBS1x} had little variation across measurement configurations. ρ^{PE} was larger in 1/10x than 1x PBS and neither concentration showed high variability. bAdult-ρ^{OC} was greater than bCalf-ρ^{OC}, consistent with impedance measurements. For both groups, ρ^{ScP+TB} was larger than ρ^{OC} with increased magnitude at 1/10x PBS. bAdult-ρ^{ScP+TB} was much larger than bCalf-ρ^{ScP+TB} at both concentrations. ρ^{AC} had average values near 0 for both groups at both concentrations and high variability for each calculated value.

Table 2.3: Raw and adjusted impedance data for mature and immature bovine tissue in high and low concentration PBS at 1kHz. Data are shown as mean ± SD. P-values denote hypothesis test comparing between relevant groups ($p<0.05$). Two values for PBS impedance are shown due to different measurement configurations for bAdult and bCalf. Background configurations are denoted by labels from Figure 2.1.

A) Raw Data as collected [Ω]

	PBS 1x			PBS 1/10x		
	bAdult	**bCalf**	**p-value**	**bAdult**	**bCalf**	**p-value**
L^{TubeA} [mm]	9.5	13.3	-	9.5	13.3	-
Bkgd (A)	534 ± 13	601 ± 8	-	3,799 ± 101	5,253 ± 154	-
Bkgd + PE (B)	780 ± 39	-	-	7,131 ± 193	6,957 ± 284	-
OC	2,304 ± 820 (A)	743 ± 27 (A)	<0.001	-	-	-
AC	741 ± 29 (B)	708 ± 17 (A)	<0.05	6,583 ± 362 (B)	4,345 ± 366 (A)	<0.001
ScP+TB	2,582 ± 995 (B)	726 ± 31 (B)	<0.001	17,675 ± 6,302 (B)	6,353 ± 614 (B)	<0.001

B) Adjusted for Background [Ω]

	PBS 1x			PBS 1/10x		
	bAdult	**bCalf**	**p-value**	**bAdult**	**bCalf**	**p-value**
L^{TubeA} [mm]	9.5	13.3	-	9.5	13.3	-
OC	1,770 ± 764	141 ± 29	<0.001	-	-	-
AC	-39 ± 59	63 ± 17	<0.03	-548 ± 365	-908 ± 338	<0.05
ScP+TB	1,802 ± 1017	83 ± 25	<0.001	10,718 ± 6,205	-604 ± 680	<0.001

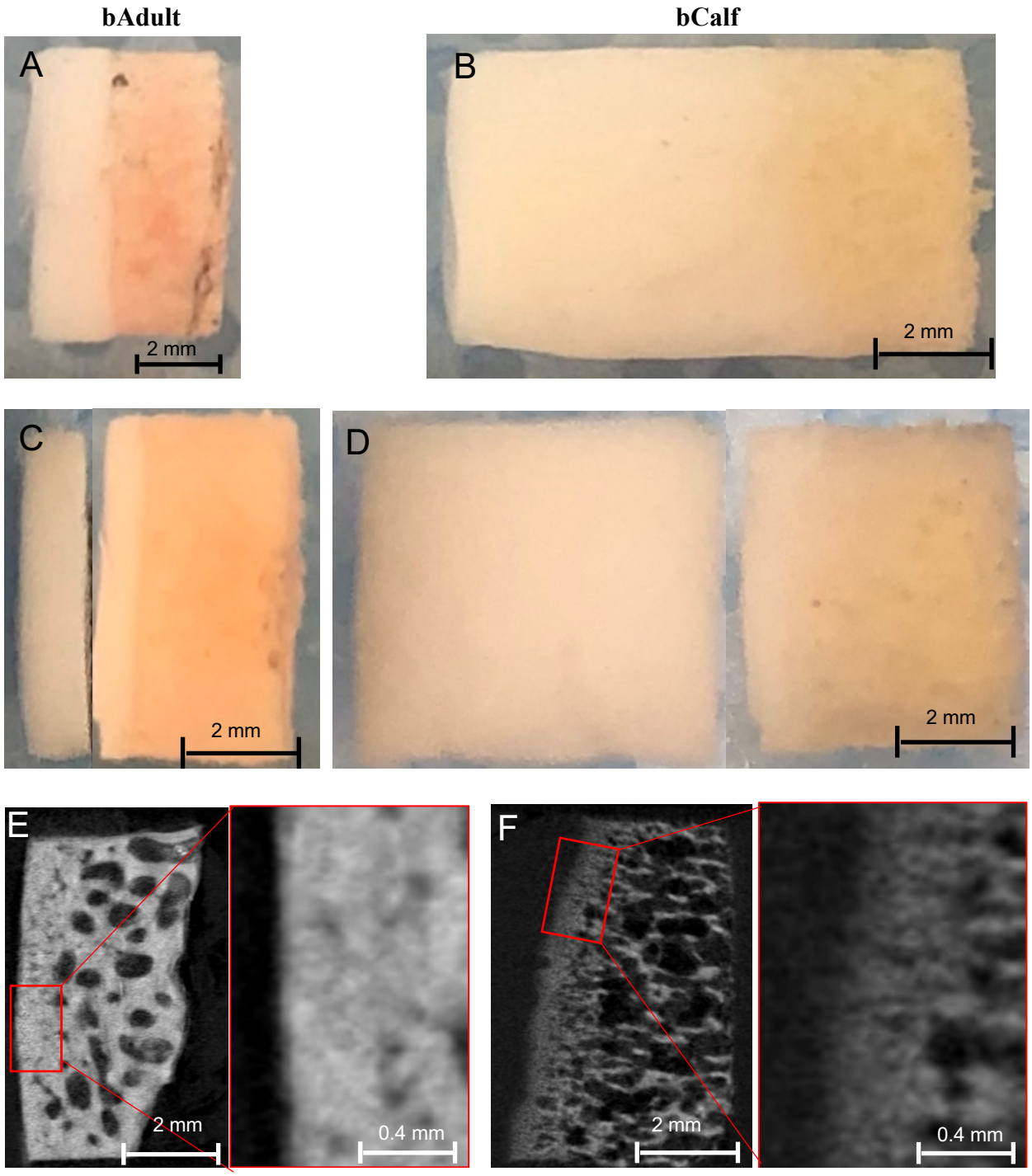

Figure 2.4: Representative (A-D) gross and (E, F) µCT images of (A, C, D) bAdult and (B, D, F) bCalf osteochondral cores. (A, B) show whole, intact osteochondral cores. (C, D) show cores post-sectioning, and (E, F) show the osteochondral interface of representative whole cores with 5x zoom.

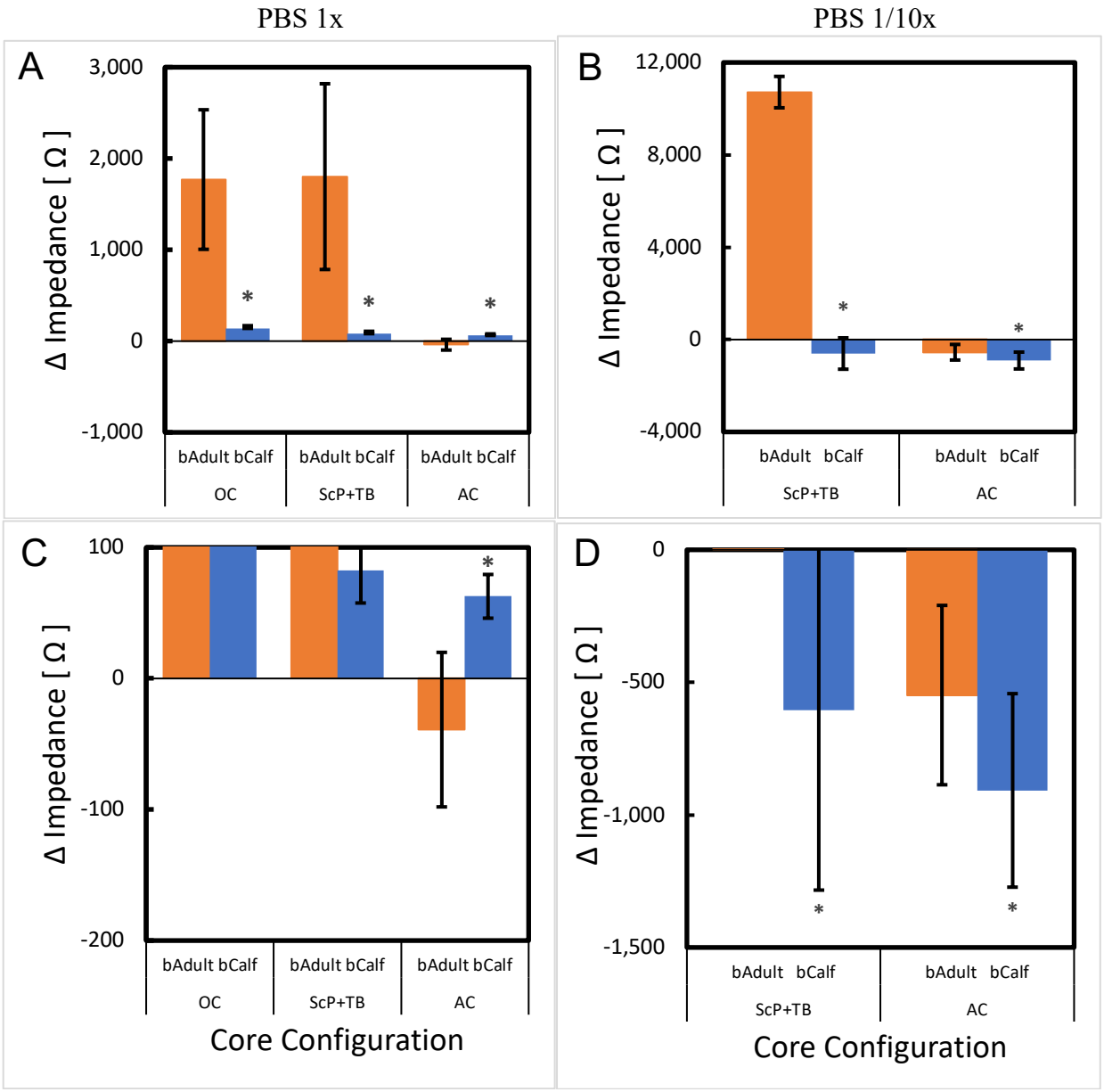

Figure 2.5: Effect of maturation on impedance across bovine OC core. bCalf and bAdult. Impedances are shown for whole, intact cores as well as the trabecular bone and subchondral plate as one measurement, and the articular cartilage. Data shown are mean ± SD, n=9. * Indicates $p<0.05$ by unpaired t-test for bAdult compared to bCalf. Measurements taken at 1kHz are shown above. Measurement solution was (A, C) PBS 1x, (B, D) PBS 1/10x. Panels (A, B) show all data, panels (C, D) show axes adjusted for AC data. Data as shown was adjusted for background impedance for each measurement set up— background impedance as measured was subtracted from tissue measurements to better illustrate differences between whole core and subcomponent measurements.

Table 2.4: Calculated resistivities (ρ) for bovine tissue from reservoir system measurements. Results shown were calculated from raw data collected at 1kHz. Data are shown (in Ω·m) as mean ± SD. Resistivity measurement results from experiment 1 were used for calculation of resistivities for configurations B-E.

		1x PBS		1/10x PBS	
Config.	**Sample**	**bAdult**	**bCalf**	**bAdult**	**bCalf**
B	**PE**	2.00 ± 0.24	-	6.03 ± 1.13	-
C	**OC**	1.71 ± 0.33	0.90 ± 0.15	-	-
D	**AC**	-0.77 ± 1.96	0.82 ± 0.06	-10.96 ± 8.92	1.60 ± 1.26
E	**ScP+TB**	11.01 ± 4.86	1.27 ± 0.13	67.67 ± 29.88	2.63 ± 2.62

Impedance of Normal and Osteoarthritic Human Osteochondral Cores. Figure 2.6 shows representative images for each tissue type, NL-hAdult and OA-hAdult. The relative dimensions between tissue types were consistent. The articular cartilage component of the OA tissue was visibly degraded at the surface. Analysis of the subchondral plate and trabecular bone via μCT imaging shows the osteochondral interface (Figure 2.6 E, F). The bony portions of the OCs are shown in white, and the AC appears black. The NL-hAdult ScP is well defined and dense, as expected (Figure 2.6 E). The OA-hAdult ScP is visibly thickened, as shown in Figure 2.6 F.

Table 2.5 shows the summary data collected for 1kHz impedance measurements made in PBS 1x—both raw data, and data corrected for background impedance from the reservoir system are shown. Figure 2.7 A and C illustrates the measured impedances for NL-hAdult and OA-hAdult tissue in PBS 1x at 1kHz. For all measured frequencies (100 Hz, 1kHz, and 10kHz) there was no difference between OA-hAdult and NL-hAdult Z^{OC} ($p=0.12$). OA-hAdult-Z^{OC} was 92%of NL-hAdult-Z^{OC}. After sectioning, it was found that the main source of the osteochondral core's impedance was due to the ScP+TB component (99% of NL-hAdult, 100% of OA-hAdult summed subcomponents). There was no significant difference between OA-hAdult-Z^{ScP+TB} and NL-hAdult-Z^{ScP+TB}. OA-hAdult Z^{ScP+TB} was 106 ± 58% of N-hAdult-Z^{ScP+TB}. The Z^{AC} values were close to that of the background measurements with some samples being slightly below the background impedance and some slightly above. There was variation between measurements within the same tissue type, with the highest variation occurring in the subchondral plate, and the lowest variation in the articular cartilage.

To better accentuate the effects of FCD on cartilage impedance, measurements were repeated on sectioned tissue in lower salt concentration (PBS 1/10x). Impedance measurements at this concentration are shown in Figure 2.7 B and D. For the Z^{ScP+TB} measurements, the magnitude

of impedance increased, as expected. After equilibration in a volume (2ml) of 1/10x, Z^{ScP} was 123% of OA-hAdult and 119% NL-hAdult subcomponent totals.. As for the Z^{AC}, an impedance value lower than that of the background was observed. With the low concentration of ions in solution, the FCD of the AC conducts the current. Between groups, there was no significant difference in impedance ($p=0.94$ at 1 kHz). For the low concentration solution, the Z^{ScP+TB} measurements continued to have the highest variation, while the Z^{AC} was generally consistent between measurements.

Resistivities were calculated for human tissue based on derived equations and impedance measurements. Results are summarized below in Table 2.6. ρ^{PBS} had values very similar to those calculated based on bovine measurements. Little variation was shown for ρ^{PE} measurements at low or high concentration PBS, and the low concentration PBS ρ^{PE} was greater than those of the high concentration PBS. Following trends in impedance measurements, ρ^{OC} between NL-hAdult and OA-hAdult groups showed enough variation that no clear conclusions can be drawn comparing the two groups. ρ^{AC} for both groups was near zero with high variation at 1x PBS and calculated to be negative at 1/10x PBS. ρ^{ScP+TB} was larger than that of ρ^{OC} for both groups, but again no clear difference for ρ^{ScP+TB} between groups. The magnitude of this was amplified at 1/10x PBS.

Table 2.5: Raw and adjusted impedance data for human osteochondral cores at 1kHz in high and low concentration PBS. Data are shown as mean ± SD. P-values denote relevant hypothesis tests comparing between groups ($p<0.05$). One PBS value is shown for NL-hAdult and OA-hAdult due to single PBS measurement across both groups in the same configuration. Measurement configurations are denoted by labels from Figure 2.1.

A) Raw Data (as Collected) [Ω].

	1x PBS			1/10x PBS		
	NL-hAdult	**OA-hAdult**	**P-value**	**NL-hAdult**	**OA-hAdult**	**P-value**
L^{TubeA} [mm]	**9.5**	**9.5**	**-**	**9.5**	**9.5**	**-**
PBS (A)	568 ± 9	562 ± 10	-	3,799 ± 101		-
Bgkd (with PE) (B)	797 ± 16	804 ± 23	-	7,431 ± 137	7,505 ± 89	-
OC	2,314 ± 546 (A)	2,029 ± 427 (A)	0.24	-	-	-
AC	810 ± 35 (B)	817 ± 35 (B)	0.67	6,401 ± 298 (B)	6,374 ± 213 (B)	0.83
ScP+TB	2,508 ± 850 (B)	2,376 ± 517 (B)	0.70	15,636 ± 4,207 (B)	15,802 ± 4,300 (B)	0.94

B) Data Adjusted for Background [Ω].

	1x PBS			1/10x PBS		
	NL-hAdult	**OA-hAdult**	**p-value**	**NL-hAdult**	**OA-hAdult**	**p-value**
L^{TubeA} [mm]	**9.5**	**9.5**	**-**	**9.5**	**9.5**	**-**
OC	1,747 ± 546	1,467 ± 431	0.12	-	-	-
AC	13 ± 29	13 ± 41	0.99	-1,029 ± 307	-1,130 ± 210	0.43
ScP+TB	1,711 ± 843	1,572 ± 518	0.67	8,206 ± 4,282	8,297 ± 4,281	0.96

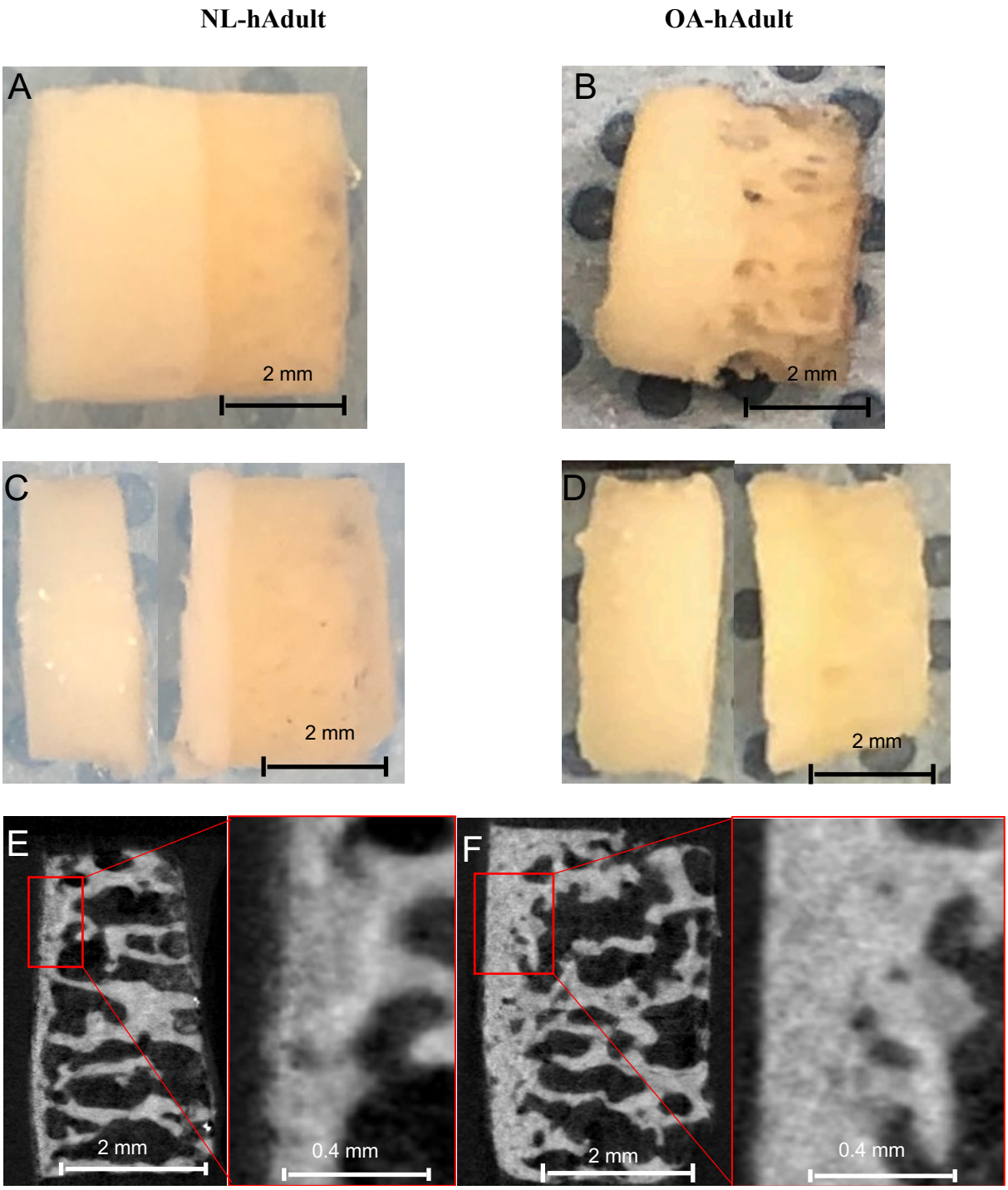

Figure 2.6: Representative (A-D) gross and (E, F) µCT images of (A, C, D) normal (NL-hAdult) and (B, D, F) osteoarthritic (OA-hAdult) osteochondral cores. (A, B) show whole, intact osteochondral cores. (C, D) show cores post-sectioning, and (E, F) show the osteochondral interface of representative whole cores with 5X zoom.

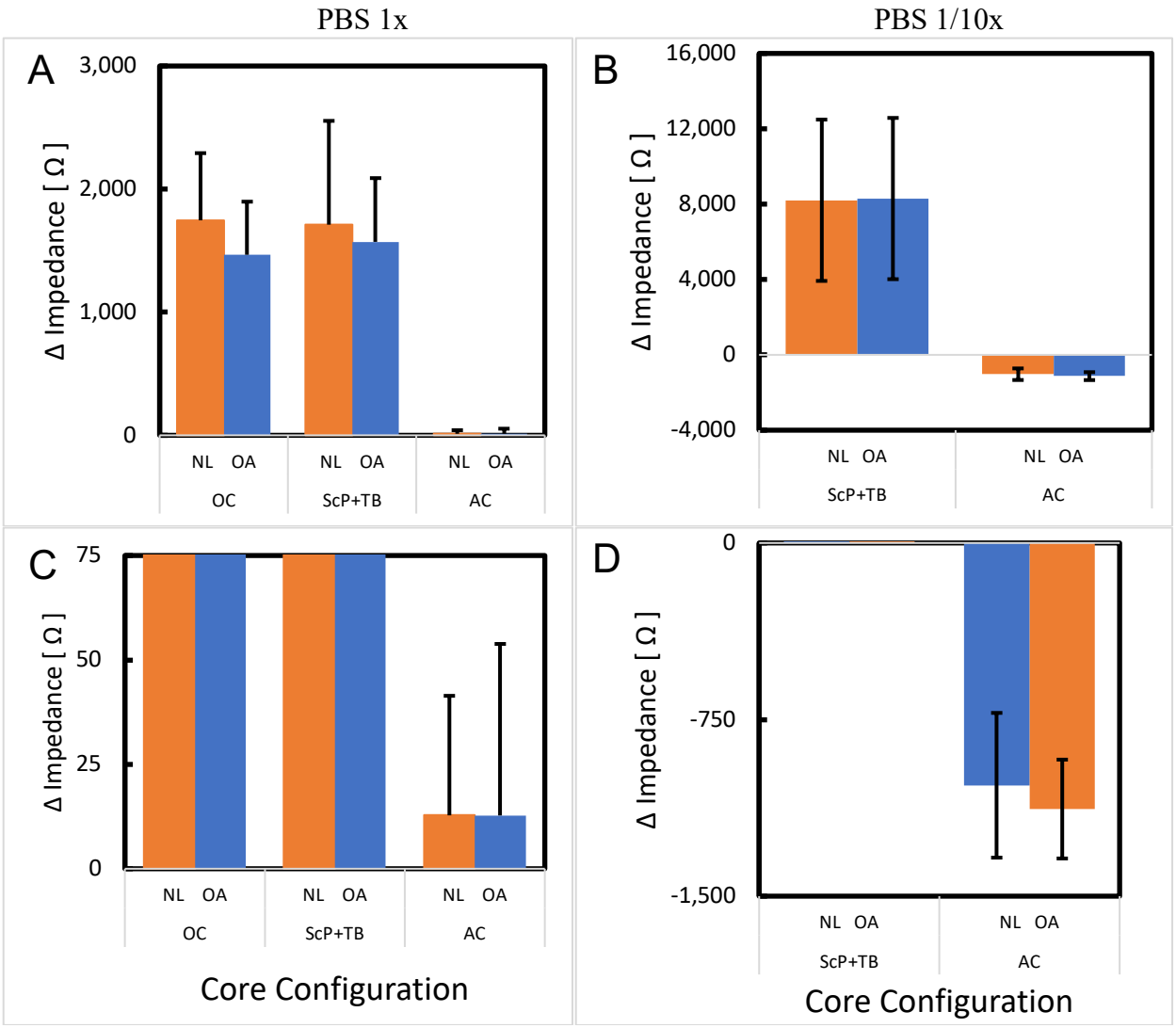

Figure 2.7: Effect of degeneration with Osteoarthritis on impedance across human OC core. Normal (NL-hAdult) and osteoarthritic (OA-hAdult). Impedances are shown for whole, intact cores as well as the trabecular bone and subchondral plate as one measurement, and the articular cartilage. Data shown are mean ± SD, n=9. Measurements shown are at 1kHz. Measurement solution was (A, C) PBS 1x, (B, D) PBS 1/10x. Panels (A, B) show all data, panels (C, D) show axes adjusted for AC data. Data as shown was adjusted for background impedance for each measurement set up— background impedance as measured was subtracted from tissue measurements to better illustrate differences between whole core and subcomponent measurements

Table 2.6: Calculated resistivity for human sample measurements made in reservoir system at 1kHz in high and low PBS concentration. Data are shown (in Ω ·m) as mean ± SD. Resistivity measurement results from experiment 1 were used for calculation of resistivities for configurations B-E.

		PBS 1x		PBS 1/10x	
Config	**Content**	**NL-hAdult**	**OA-hAdult**	**NL-hAdult**	**OA-hAdult**
A	**PBS**	0.79 ± 0.01	0.79 ± 0.02	5.36 ± 0.14	5.36 ± 0.14
B	**PE**	2.90 ± 0.09	2.99 ± 0.14	26.82 ± 1.10	27.64 ± 0.54
C	**OC**	8.98 ± 2.77	4.98 ± 1.06	-	-
D	**AC**	0.96 ± 0.71	0.68 ± 0.45	-25.53 ± 7.78	-5.14 ± 2.65
E	**ScP+TB**	10.50 ± 3.86	8.14 ± 2.41	55.25 ± 28.80	44.17 ± 19.89

2.6 DISCUSSION

The above results established an approach for assessing the electrical impedance (Z) across fluid and tissue samples, including cylindrical OCs, and used the approach to delineate variations in Z with OC development and deterioration. Since ΔZ was determined for tissue samples relative to bath solutions, and rho depended on rho bath solution as well as delta Z and tissue geometry, it was important to verify the former, as was done in Exp 1 (call out Tables and Figures). Since the OCs evaluated here had a small portion of subchondral TB, the effect of the marrow component within the TB was reduced by centrifugation (Exp 2, call out Tables and Figures) (2) In 1x PBS, the Z of mature bovine (Exp 3) and human (Exp 4) OCs was almost an order of magnitude higher than that of immature bovine OCs. Sub-dividing OCs identified the ScP+TB portion, rather than the AC portion, as the major contributor to OC impedance. In 1/10x PBS, the major contribution of Z ScP+TB to Z OC was still evident, with large magnitude impedances and resistivities. The impedance values were similar at the 100 Hz, 1 kHz, and 10 kHz test frequencies that were standard to the equipment used.

In experiment 1, resistivity of PBS, ρ^{PBS}, was determined to be estimates 0.570 ± 0.002 Ω·m and 4.99 ± 0.08 Ω·m for 1x and 1/10x, respectively. These values are consistent (within x %) with the theoretically predicted values shown in Table 1-2. Slight differences between the values determined here, and those predicted theoretically, may be due to slight inaccuracies in dimensions used for normalization. For example, variation in the tube diameter by the stated tolerance of ** could lead to an x% imprecision in the resistivity estimate. The computed values were used for all resistivity calculations due to their consistency with theoretical predictions.

Marrow removal reduces impedance of osteochondral cores, with the most significant effect in immature tissue. Experiment 2 established that the presence of bone marrow increases

the overall impedance of an immature bovine osteochondral core. It was also established that immature bovine osteochondral cores had the lowest overall impedance, therefore the effect of bone marrow is likely the largest magnitude change in immature tissue. Due to the differences in magnitude of immature bovine tissue impedance relative to adult bovine or human tissue, the magnitude of this effect likely varies. For future studies investigating the impedance or resistivity of osteochondral tissue the marrow should be removed for improved accuracy. Marrow resistivity was calculated to be ~1.15 Ω·m. This was higher than that of PBS and cartilage samples as expected, but this value was lower than that of previous literature studies. Balmer (2018) calculated bone marrow resistivity to be 4.3 Ω·m. Resistivity of bone marrow could be better understood using a larger volume of trabecular bone and bone marrow.

Bovine osteochondral tissue has an increased impedance with maturation, with the subchondral plate as the main source of the impedance increases. Experiment 3 established that bAdult tissue has a higher overall impedance than bCalf tissue. There was no significant difference between the impedance of the overall OC and the impedance of the sectioned subchondral plate and trabecular bone subcomponents within corresponding age groups (bCalf, bAdult). The subchondral plate is the major source of impedance for the whole OC, especially in mature bovine tissue and less so in immature tissue. The increase in impedance of the OC is consistent with the formation of the subchondral plate. Measurements in PBS 1/10x were repeated for a smaller section of samples after approximately two weeks after equilibrating tissue in a larger volume of solution. This allowed any additional ions in tissue from PBS 1x to desorb into the larger volume of solution to reduce conductance of the tissue. Values that were initially lower than background impedance measured were now slightly larger than the corresponding background. This could have been due to ions desorbing from the tissue, or general breakdown of the tissue over time.

The subchondral plate was the main source of impedance for human tissue, but there was no difference overall between OA and NL samples due to high tissue variability. When impedance of sections of the human tissue was compared to the impedance of the subchondral plate and trabecular bone, there was no difference—demonstrating that changes to the whole OC impedance are driven by changes to the subchondral plate. When the samples were compared by condition (Normal vs Osteoarthritic) no difference was found. This is likely due to the variability in both the subchondral plate and the articular cartilage—the simultaneous increased thickness and porosity of the subchondral plate could have confounding effects on impedance as OA degenerates the tissue. The concurrent advancement of the tidemark into the articular cartilage, increases the mineralized component of the ScP region. This thickening of the ScP would reduce any effect of increased porosity on the impedance of the tissue.

System specific impedance measurements were converted to resistivity values to compare differences in tissue more accurately. The resistivity of PBS 1x, ρPBS, was theoretically predicted to be 0.58 Ω·m, whereas it was measured to be 0.79 Ω·m in experiment 4. This could be contributed to the impedance due to the electrodes which was not accounted for in resistivity calculations, unlike in experiment 1. A study by Hasegawa (1983) found that articular cartilage in Ringer's solution, ρ^{AC} is 1.30 Ω·m. This value is larger than that of bCalf-ρ^{AC} determined in this study (0.90±0.15 Ω·m). These differences may be due to the tissue source. In 1/10x PBS solution, the bCalf was found to have a lower impedance than that measured for the background. This is consistent with the Donnan effect, in that the free Na^+ ions in solution concentrate within the tissue and increase the conductance. Resistivity for bAdult AC in this study was calculated as -0.77 ± 1.96 Ω·m. The thin cartilage samples and background subtraction likely contributed to imprecision of the articular cartilage resistivity calculations. The resistivity of the subchondral plate and

trabecular bone component, ρ^{ScP+TB}, was calculated to be ~11 Ω·m for bAdult samples. This is consistent with results from Balmer (2018), in which the resistivity of mature bovine cortical bone was calculated to be ~110 Ω·m, when considering the additional trabecular bone component of the ScP+TB samples in this study [2]. Overall, for each tissue group the ρ^{ScP+TB} was the largest, confirming that the subchondral plate is the main source of impedance throughout osteochondral tissue samples.

Generally, the results presented in this study provide further insight into basic physical properties-- resistivity and conductivity-- of the osteochondral interface. Impedance measurements can be a simple nondestructive index of osteochondral tissue. Utilizing impedance measurements of osteochondral cores and their subcomponents is a relatively quick and repeatable method of characterizing important structures after various possible *in vitro* manipulations as well as throughout maturation.

2.7 ACKNOWLEDGEMENTS

I would like to thank Dr. William D Bugbee for making available human tissue remnants from his orthopaedic surgeries. I would also like to thank Dr. Albert C Chen for her help with μCT imaging and Van Wong for his help with reservoir fabrication.

Chapter 2, in part is currently being prepared for submission for publication of the material. Bullard, Caroline G; Wong, Van W; Chen, Albert C; Masuda, Koichi; Bugbee, William D; Sah, Robert L. The thesis author was the primary investigator and author of this material.

2.7 REFERENCES

1. Amini M., Hisdal J., Kalvøy H., "Applications of bioimpedance measurement techniques in tissue engineering," JoEB, vol. 9, pp. 142-158, 2018.

2. Balmer T. W., Vesztergom S., Broekmann P., Stahel A., Büchler P., "Characterization of the electrical conductivity of bone and its correlation to osseous structure," Sci Rep, vol. 8, p. 8601, 2018

3. Burr D. B., Gallant M. A., "Bone remodelling in osteoarthritis," Nat Rev Rheumatol, vol. 8, pp. 665–673, 2012

4. Fan X., Wu X., Crawford R., Xiao Y., Prasadam I., "Macro, micro, and molecular changes of the osteochondral interface in osteoarthritis development," Front Cell Dev Biol, vol. 9, 2021

5. Fazeli P. K., Horowitz M.C., MacDougald O.A., Scheller E.L., Rodeheffer M.S., Rosen C.J., Klibanski A., "Marrow fat and bone—new perspectives," J Clin Endocrinol Metab, vol. 98, pp. 935–945, 2013

6. Gandhi N. S., Mancera R.L., "The structure of glycosaminoglycans and their interactions with proteins," Chem Biol Drug Des, vol. 72, pp. 455–482, 2008

7. Goldring S.R., Goldring M.B., "Changes in the osteochondral unit during osteoarthritis: structure, function and cartilage–bone crosstalk," Nat Rev Rheumatol, vol. 12, pp. 632–644, 2016

8. Gurkan, U.A., Akkus, O., "The mechanical environment of bone marrow: a review," Ann Biomed Eng, vol. 36, pp 1978-1991, 2008

9. Hasegawa I., Kuriki S., Matsuno S., Matsumoto G., "Dependence of electrical conductivity on fixed charge density in articular cartilage," Clin Orthop Relat Res, pp. 283–288, 1983

10. Hoemann C., Lafantaisie-Favreau C.-H., Lascau-Coman V., Chen G., Guzmán-Morales J., "The cartilage-bone interface," J Knee Surg, vol. 25, pp. 085–098, 2012

11. Hwang J., Bae W. C., Shieu W., Lewis C.W., Bugbee W.D., Sah R.L., "Increased Hydraulic Conductance of Human Articular Cartilage and Subchondral Bone Plate with Progression of Osteoarthritis," Arthritis Rheum, vol. 58, pp. 3831–3842, 2008

12. Hwang J., "Integration of cartilage and bone through a calcified cartilage interface to form a functional osteochondral graft,"[PhD Thesis] UC San Diego, 2010

13. Lesperance L. M., Gray M. L., Burstein D., "Determination of fixed charge density in cartilage using nuclear magnetic resonance," J. Orthop. Res., vol. 10, pp. 1–13, 1992

14. Madry H., van Dijk C. N., Mueller-Gerbl M., “The basic science of the subchondral bone,” Knee Surg Sports Traumatol Arthrosc, vol. 18, pp. 419–433, 2010

15. Maroudas A., Muir H., “The correlation of fixed negative charge with glycosaminoglycan content of human articular cartilage,” Biochimica Biophys Acta Gen Subj, vol. 177, pp. 492–500, 1969

16. Naung N.Y., Suttapreyasri S., Kamolmatyakul S., Nuntanaranont T., “Comparative study of different centrifugation protocols for a density gradient separation media in isolation of osteoprogenitors from bone marrow aspirate,” J Oral Biol Craniofac Res, vol. 4, pp. 160–168, 2014

17. Oftadeh R., Perez-Viloria M., Villa-Camacho J. C., Vaziri A., Nazarian A., “Biomechanics and mechanobiology of trabecular bone: a review,” J Biomech Eng, vol. 137, pp. 0108021–01080215, 2015

18. Schmidt, T.A., “Proteoglycan 4 metabolism and boundary lubrication of articular cartilage.” [PhD Thesis] University of California, San Diego, 2006.

19. Sophia Fox A.J., Bedi A., Rodeo S.A., “The basic science of articular cartilage: structure, composition, and function,” Sports Health, vol. 1, pp. 461–468, 2009

20. Taheri S.,Winkler T. , Schenk L.S., Neuerburg C.,.Baumbach S.F, Zustin J., LehmannW., Schilling A.F, “Developmental transformation and reduction of connective cavities within the subchondral bone,” Int J Mol Sci, vol. 20, p. 770, 2019

21. Yuan X.L., Meng H.Y., Wang Y.C., Peng J., Guo Q.Y., Wang A.Y, Lu S.B.,“Bone-cartilage interface crosstalk in osteoarthritis: potential pathways and future therapeutic strategies” Osteoarthritis Cartilage vol. 22, pp. 1077–1089, 2014

CHAPTER 3

CONCLUSIONS

3.1 Summary Of Findings

In the execution of this study, it was first confirmed that the presence of bone marrow affects the overall impedance of osteochondral tissue. Removal of bone marrow increases the accuracy of the impedance measurements to the osteochondral components and is a beneficial pre-treatment step that should be used in future studies of a similar nature. Next, normal skeletal maturation of bovine tissue was established to significantly increase the impedance of a whole osteochondral core across a range of frequencies. Subsequent sectioning and analysis determined that the primary source of osteochondral tissue impedance is from the subchondral plate. Resistivity calculations confirmed that the subchondral plate provides the most impedance for both tissue groups, but the signal is much stronger for mature tissue. Finally, normal human tissue was compared to human osteoarthritic tissue. No statistically significant difference was observed with a p value > 0.05, however previous studies have shown a difference in impedance—therefore more investigation is necessary to make conclusions about the relationship between OA and OC impedance. sectioning, it was determined that the largest contributor to OC impedance was still the subchondral plate for both normal and osteoarthritic tissue.

3.2 Discussion

Data from experiments 1, 2, and 3 of study of this project generally followed expected results. For the comparison of normal and osteoarthritic human tissue, there may have been confounding variables at play which had opposing effects, preventing statistically significant conclusions. The ScP may have thickened in such a way that the effects of the mineralized components overrode the effects of the increased porosity of the subchondral plate. The tissue of the osteochondral interface is also highly variable, and though all tissue was harvested from the

femoral condyles, there may have been unpredicted variation between regions within the femoral condyles which contributed to the differences observed in this study.

3.3 Future Work

In the short term, performing high resolution imaging of similar tissue at the osteochondral interface, including DVI and μCT imaging, and determining if there is a correlation between measured impedance and the thickness and porosity of the subchondral plate can elucidate the differences in results from this study, and previous work performed comparing normal and osteoarthritic tissue. Furthermore, performing GAG quantification on the articular cartilage and correlating that more specifically to the measured impedance of the tissue will provide further insight into the variation from expectations of this study.

In the long term, the implications of this study are broad reaching. Impedance measurements are simple, non-destructive, and fast measures that can provide information about the structure of various tissues. It provides a possible in vitro methodology for various tissue engineering applications, and in combination with other techniques particularly useful at characterizing both molecular and structural changes of tissues relevant to disease progression in the articular joint.

APPENDIX

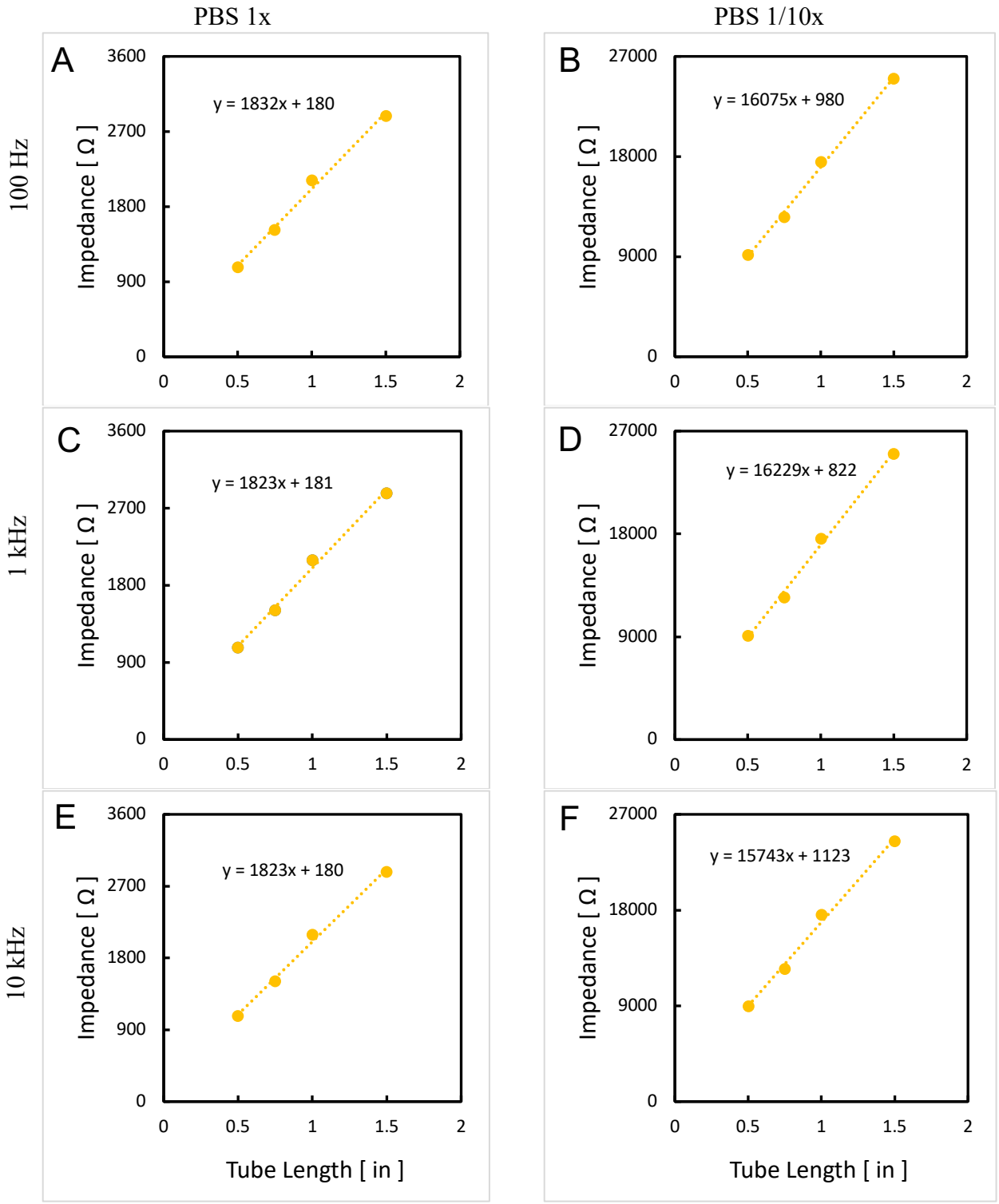

Supplemental Figure-1: Linear regression analysis of impedance over various tube lengths. Data in the column on the left was measured in PBS 1X, data in the column on the right was measured in PBS 1/10X. Panels (A, B) were measured at 100Hz. Panels (C, D) were measured at 1kHz. Panels (E, F) were measured at 100Hz. Data was averaged from three pairs of electrodes.

Supplemental Table-1: Raw and Adjusted Summary Data for Impedance Measurements of Bovine Osteochondral Cores in PBS 1x. Data are shown as mean ± SD. Background measurements were made with polyethylene (PE) supports to hold tissue in place. Background configurations are denoted by labels from Figure 2.1.

A) Raw Data (as collected) [Ω]

	bAdult			**bCalf**		
Length^{TubeA} [mm]	9.5			13.2		
Freq.	**100Hz**	**1kHz**	**10kHz**	**100Hz**	**1kHz**	**10kHz**
PBS	563 ± 8	542 ± 9	528 ± 9	667 ± 8	643 ± 8	633 ± 8
Bgkd (With PE)	804 ± 40	780 ± 39	771 ± 38	667 ± 8	644 ± 8	633 ± 8
OC	2,337 ± 766 (A)	2,304 ± 743(A)	2,289 ± 734(A)	816 ± 25(A)	820 ± 27(A)	816 ± 25(A)
AC	761 ± 26 (B)	741 ± 29 (B)	728 ± 28 (B)	733 ± 15 (A)	708 ± 17 (A)	701 ± 18 (A)
ScP+TB	2,606 ± 987(B)	2,582 ± 995(B)	2,546 ± 989 (B)	748 ± 28 (B)	726 ± 31 (B)	716 ± 29 (B)

B) Data Adjusted for Background Impedance

	bAdult			**bCalf**		
Length^{TubeA} [mm]	9.5			13.2		
Freq.	**100Hz**	**1kHz**	**10kHz**	**100Hz**	**1kHz**	**10kHz**
OC	1,785 ± 809	1,770 ± 764	1,764 ± 809	146 ± 25	141 ± 29	138 ± 25
AC	-43 ± 55	-39 ± 59	-42 ± 58	65 ± 17	63 ± 17	66 ± 18
ScP+TB	1,802 ± 1,007	1,802 ± 1,017	1,775 ± 1,009	81 ± 24	83 ± 25	82 ± 25

Supplemental Table-2: Raw and Adjusted Summary Data for Impedance Measurements of Bovine Osteochondral Cores in PBS 1/10x. Data are shown as mean ± SD. Background measurements were made with polyethylene (PE) supports to hold tissue in place. Background configurations are denoted by labels from Figure 2.1.

A) Raw Data (as collected) [Ω]

	bAdult			**bCalf**		
Length^{TubeA} [mm]	9.5			13.2		
Freq.	**100 Hz**	**1 kHz**	**10kHz**	**100 Hz**	**1kHz**	**10kHz**
PBS (A)	3,830 ± 95	3,799 ± 101	3,892 ± 321	5,281 ± 159	5,253 ± 154	5,211 ± 152
Bgkd (With PE) (B)	7,197 ± 207	7,131 ± 193	7088 ± 194	7,012 ± 297	6,957 ± 284	6,917 ± 294
AC	6,617 ± 360 (B)	6,583 ± 362 (B)	6,522 ± 372 (B)	4,388 ± 358 (A)	4,345 ± 366 (A)	4,314 ± 357 (A)
ScP+TB	17,815 ± 6,368 (B)	17,675 ± 6,302 (B)	17,268 ± 6,016 (B)	6,382 ± 586 (B)	6,353 ± 614 (B)	6,286 ± 583 (B)

B) Data Adjusted for Background [Ω]

	bAdult			**bCalf**		
Length^{TubeA} [mm]	9.5			13.2		
Freq.	**100 Hz**	**1kHz**	**10kHz**	**100 Hz**	**1kHz**	**10kHz**
AC	-581 ± 364	-548 ± 365	-565 ± 367	-894 ± 359	-908 ± 338	-897 ± 353
ScP+TB	10,804 ± 6,269	10,718 ± 6,205	10,350 ± 5,902	-630 ± 693	-604 ± 680	-631 ± 691

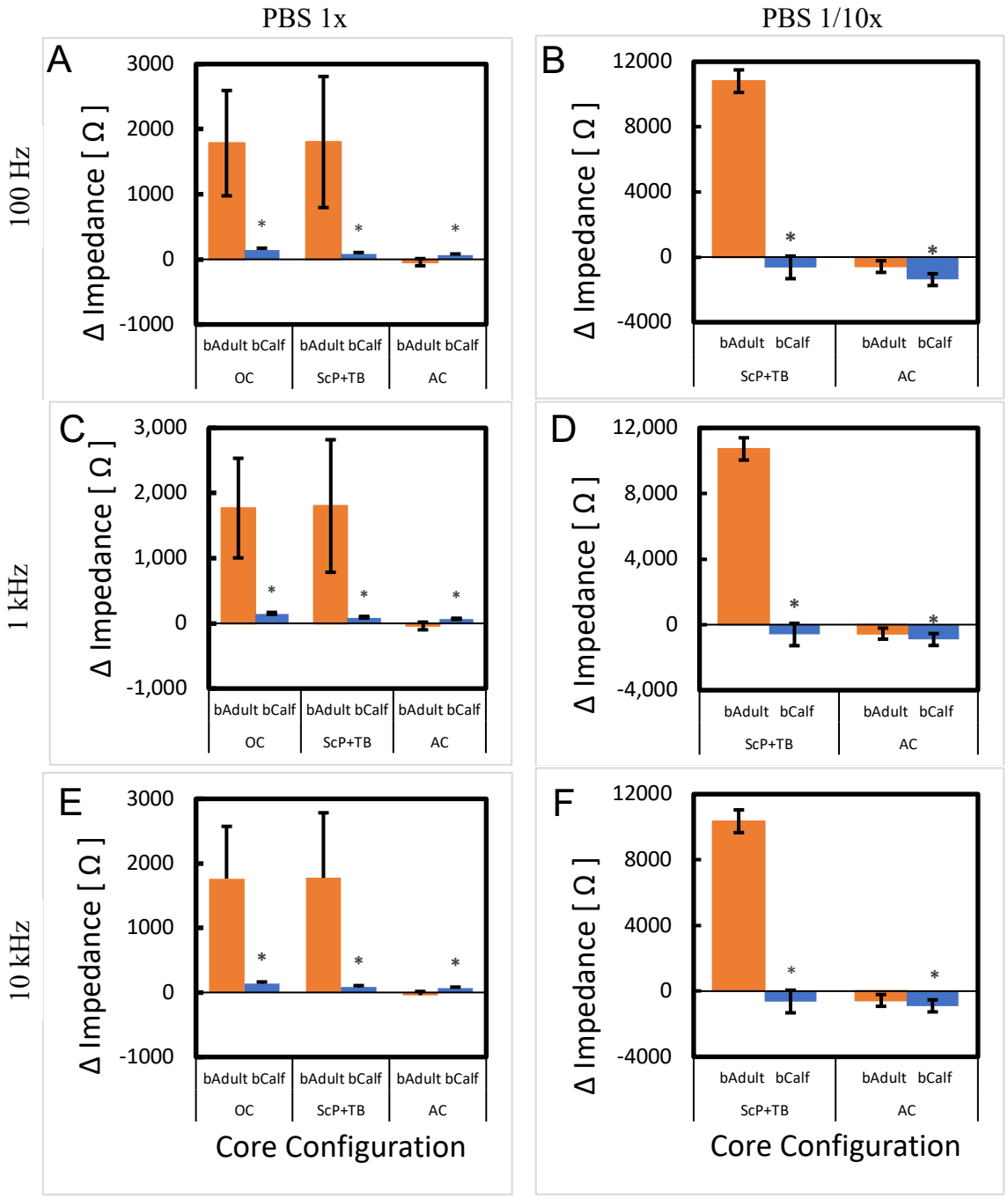

Supplemental Figure-2: Effect of maturation on impedance across bovine OC core. bCalf and bAdult. Impedances are shown for whole, intact cores as well as the trabecular bone and subchondral plate as one measurement, and the articular cartilage. Data shown are mean ± SD, n=9. * Indicates $p<0.05$ by unpaired t-test for bAdult compared to bCalf. Panels show data at different frequencies: Panels A, B: 100 Hz, Panels C, D: 1kHz, Panels E, F 10kHz. Left column shows data from PBS 1x, and right column shows data from PBS 1/10x. Data as shown was adjusted for background impedance for each measurement set up— background impedance as measured was subtracted from tissue measurements to better illustrate differences between whole core and subcomponent measurements.

Supplemental Table-3: Desorption Impedance Analysis Results. Measurements were made in 1/10x PBS after equilibration in 50mL of solution. Data are shown as mean ± SD. bAdult n=2, bCalf n=9. [Ω]

A) Raw Data

	bAdult			**bCalf**		
Length^{TubeA} [mm]	**9.5**			**9.5**		
Freq.	**1khz**	**10khz**	**100hz**	**1khz**	**10khz**	**100hz**
PBS (A)	-	-	-	4,858 ± 96	4,826 ± 109	4,891 ± 83
PBS +PE (B)	6,503 ± 624	6,456 ± 639	6,543 ± 628	6,976 ± 93	6,938 ± 89	7,019 ± 103
AC	6,810 ± 73 (B)	6,791 ± 74(B)	6,874 ± 71 (B)	5,484 ± 224 (A)	5,419 ± 221(A)	5,537 ± 222 (A)
ScP+TB	15,239 ± 4,142(B)	14,823 ± 3,854(B)	15,370 ± 4,104(B)	7,892 ± 663 (B)	7,835 ± 666(B)	7,967 ± 672(B)

B) Adjusted Data

	bAdult			**bCalf**		
Length^{TubeA} [mm]	**9.5**			**9.5**		
Freq.	**1khz**	**10khz**	**100hz**	**1khz**	**10khz**	**100hz**
AC	307 ± 551	335 ± 565	331 ± 557	626 ± 280	593 ± 286	646 ± 280
ScP+TB	8,736 ± 4765	8,367 ± 4,494	8,827 ± 4,732	916 ± 665	896 ± 665	947 ± 688

Supplemental Table-4: Average calculated resistivity from reservoir system configurations for bovine sample measurements across all frequencies. Data are shown as mean ± SD. [Ω ·m]

			1x PBS		1/10x PBS	
config	**content**	**Freq.**	**bAdult**	**bCalf**	**bAdult**	**bCalf**
A	**PBS**	**100 Hz**	0.75 ± 0.01	0.76 ± 0.01	5.40 ± 1.3	6.02 ± 0.18
A	**PBS**	**1khz**	0.73 ± 0.01	0.73 ± 0.01	5.36 ± 0.14	5.99 ± 0.18
A	**PBS**	**10khz**	0.85 ± 0.01	0.72 ± 0.01	5.49 ±0.45	5.94 ± 0.17
B	**PE**	**100 Hz**	2.02 ± 0.23	-	6.01 ± 1.13	-
B	**PE**	**1khz**	2.00 ± 0.24	-	6.01 ± ± 1.14	-
B	**PE**	**10khz**	1.40 ± 0.26	-	6.18 ± 0.33	-
C	**OC**	**100 Hz**	1.92 ± 0.33	0.90 ± 0.15	-	-
C	**OC**	**1khz**	1.71 ± 0.33	0.90 ± 0.15	-	-
C	**OC**	**10khz**	1.24 ± 0.29	0.89 ± 0.15	-	-
D	**AC**	**100 Hz**	-0.88 ± 1.84	0.82 ± 0.06	-11.98 ± 8.89	1.55 ± 1.34
D	**AC**	**1khz**	-0.77 ± 1.96	0.82 ± 0.06	-10.96 ± 8.92	1.52 ± 1.26
D	**AC**	**10khz**	-0.86 ± 1.95	0.83 ± 0.06	-11.47 ± 8.92	1.60 ± 1.31
E	**ScP+TB**	**100 Hz**	11.02 ± 4.82	1.27 ± 0.11	67.13 ± 30.15	2.57 ± 2.67
E	**ScP+TB**	**1khz**	11.00 ± 4.86	1.27 ± 0.13	66.67 ± 29.88	2.69 ± 2.62
E	**ScP+TB**	**10khz**	10.85 ± 4.86	1.28 ± 0.12	64.67 ± 28.65	2.63 ± 2.66

Supplemental Table-5: Raw and Adjusted Summary Data for Human Osteochondral Cores in PBS 1x. Data are shown as mean ± SD. Background configurations are denoted by labels from Figure 2.1.

A) Raw Data (As collected) [Ω]

	NL-hAdult			OA-hAdult		
Length^{TubeA} [mm]	9.5			9.5		
Freq.	**100 Hz**	**1 kHz**	**10 kHz**	**100 Hz**	**1 kHz**	**10 kHz**
PBS (A)	560 ± 11	568 ± 9	589 ± 11	580 ± 8	562 ± 10	556 ± 9
Bgkd (with PE) (B)	818 ± 17	797 ± 16	792 ± 15	821 ± 21	804 ± 23	796 ± 18
OC	2,364 ± 542 (A)	2,314 ± 546 (A)	2,289 ± 526 (A)	2,068 ± 442 (A)	2,029 ± 427 (A)	2,004 ± 403 (A)
AC	839 ± 36 (B)	810 ± 35 (B)	800 ± 40 (B)	833 ± 36 (B)	817 ± 35 (B)	805 ± 36 (B)
ScP+TB	2,616 ± 753 (B)	2,508 ± 850 (B)	2,532 ± 747 (B)	2,396 ± 519 (B)	2,376 ± 517 (B)	2,348 ± 516 (B)

B) Data Adjusted for Background

	NL-hAdult			OA-hAdult		
Freq.	**100 Hz**	**1 kHz**	**10 kHz**	**100 Hz**	**1 kHz**	**10 kHz**
OC	1,775 ± 542	1,747 ± 546	1,729 ± 525	1,489 ± 446	1,467 ± 431	1,449 ± 406
AC	20 ± 31	13 ± 29	8 ± 40	12 ± 41	13 ± 41	9 ± 40
ScP+TB	1,797 ± 747	1,711 ± 843	1,740 ± 741	1,575 ± 519	1,572 ± 518	1,552 ± 517

Supplemental Table-6: Raw and Adjusted Summary Data for Human Osteochondral Cores in PBS 1/10x. Data are shown as mean ± SD. [Ω]

A) Raw Data as collected

	NL-hAdult			OA-hAdult		
Length^{TubeA} [mm]	9.5			9.5		
Freq.	**100 Hz**	**1kHz**	**10kHz**	**100 Hz**	**1kHz**	**10kHz**
Bkgd (A)	3,880 ± 95	3,799 ± 101	3,892 ± 321	3,880 ± 95	3,799 ± 101	3,892 ± 321
Bkgd + PE (B)	7,489 ± 132	7,431 ± 137	7,388 ± 131	7,556 ± 70	7,505 ± 89	7,455 ± 122
AC	6,451 ± 281 (B)	6,401 ± 298 (B)	6,347 ± 273 (B)	6,411 ± 200 (B)	6,374 ± 213 (B)	6,284 ± 298 (B)
ScP+TB	15,251 ± 4,308 (B)	15,636 ± 4,207 (B)	14,928 ± 3,623 (B)	15,897 ± 4,299 (B)	15,802 ± 4,300 (B)	15,510 ± 4,156 (B)

B) Data Adjusted for Background

	NL-hAdult			OA-hAdult		
Freq.	**100 Hz**	**1kHz**	**10kHz**	**100 Hz**	**1kHz**	**10kHz**
AC	-1,038 ± 299	-1,029 ± 307	-1,041 ± 289	-1,146 ± 190	-1,130 ± 210	-1,171 ± 295
ScP+TB	7,762 ± 4,357	8,206 ± 4,282	7,540 ± 3,697	8,341 ± 4,289	8,297 ± 4,281	8,055 ± 4,151

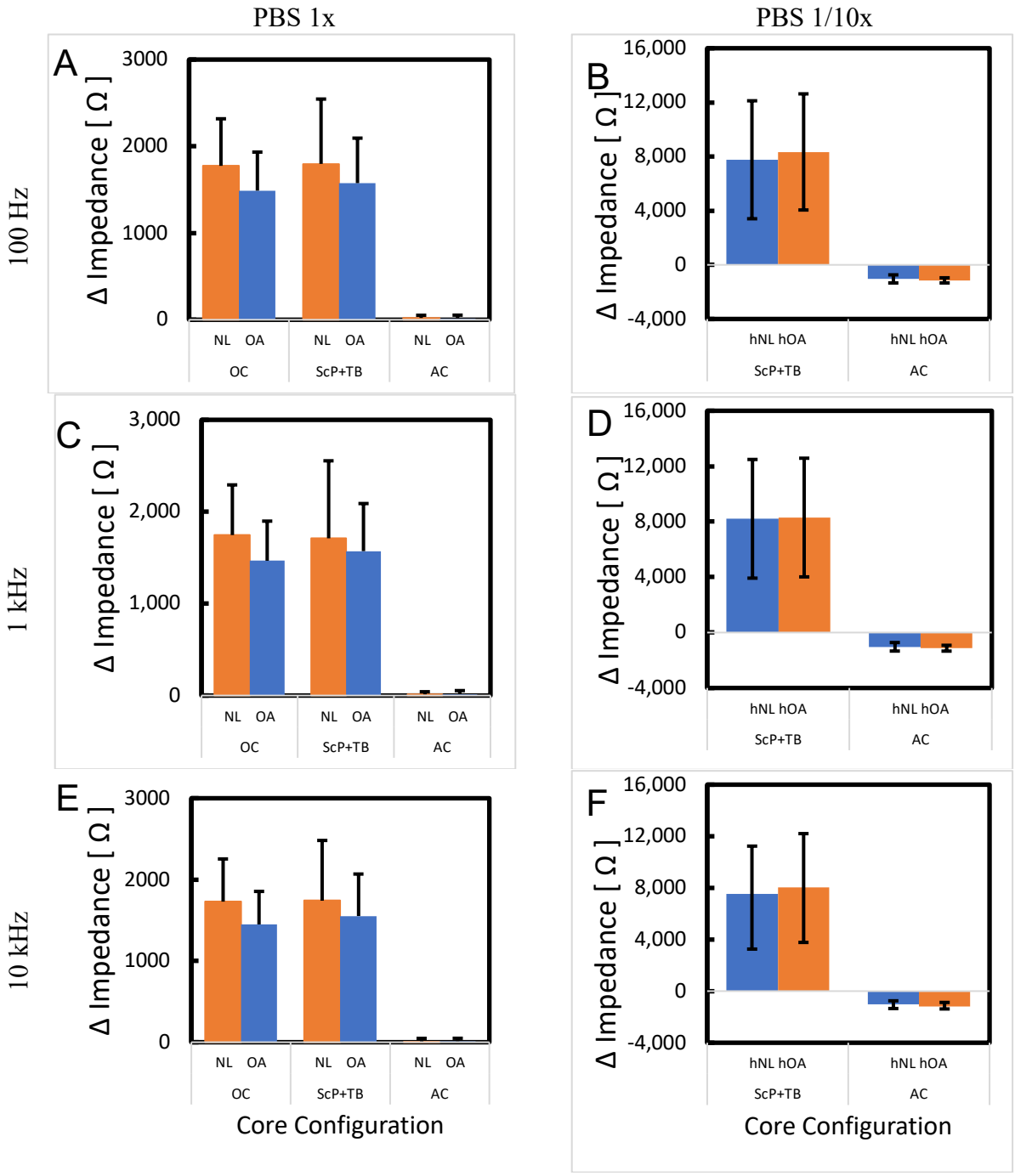

Supplemental Figure-3: Effect of degeneration on impedance across human OA core. NL-hAdult and OA-hAdult. Impedances are shown for whole, intact cores as well as the trabecular bone and subchondral plate as one measurement, and the articular cartilage. Data shown are mean ± SD, n=9. * Indicates $p<0.05$ by unpaired t-test for NL-hAdult compared to OA-hAdult. Panels show data at different frequencies: Panels A, B: 100 Hz, Panels C, D: 1kHz, Panels E, F 10kHz. Left column shows data from PBS 1x, and right column shows data from PBS 1/10x. Data as shown was adjusted for background impedance for each measurement set up— background impedance as measured was subtracted from tissue measurements to better illustrate differences between whole core and subcomponent measurements.

Supplemental Table-7: Average calculated resistivity from reservoir system human sample measurements across all frequencies. Data are shown as mean ± SD. [Ω ·m]

			1x PBS		1/10x PBS	
configuration	**content**	**Frequency**	**NL-hAdult**	**OA-hAdult**	**NL-hAdult**	**OA-hAdult**
A	**PBS**	**100 Hz**	0.82 ± 0.01	0.83 ± 0.02	5.40 ± 0.13	
A	**PBS**	**1khz**	0.79 ± 0.01	0.80 ± 0.01	5.36 ± 0.14	
A	**PBS**	**10khz**	0.78 ± 0.01	0.79 ± 0.02	5.49 ± 0.45	
B	**PE**	**100 Hz**	3.04 ± 0.10	2.22 ± 0.13	26.96 ± 1.03	27.36 ± 0.59
B	**PE**	**1khz**	2.90 ± 0.09	2.12 ± 0.14	26.82 ± 1.03	27.27 ± 0.77
B	**PE**	**10khz**	2.87 ± 0.09	2.07 ± 0.11	26.05 ± 2.10	26.45 ± 1.85
C	**OC**	**100 Hz**	8.88 ± 2.77	5.31 ± 1.09	-	-
C	**OC**	**1khz**	8.76 ± 2.78	5.21 ± 1.06	-	-
C	**OC**	**10khz**	8.68 ± 2.69	5.15 ± 1.01	-	-
D	**AC**	**100 Hz**	0.96 ± 0.71	0.94 ± 0.44	-25.87 ± 7.77	-5.51 ± 2.25
D	**AC**	**1khz**	0.85 ± 0.65	0.91 ± 0.45	-25.53 ± 7.78	-5.33 ± 2.33
D	**AC**	**10khz**	0.81 ± 0.77	0.87 ± 0.43	-25.89 ± 7.51	-5.60 ± 2.65
E	**ScP+TB**	**100 Hz**	10.50 ± 3.86	8.42 ± 2.42	52.18 ± 28.68	45.02 ± 19.57
E	**ScP+TB**	**1khz**	9.97 ± 4.43	8.37 ± 2.41	55.25 ± 28.80	44.84 ± 19.55
E	**ScP+TB**	**10khz**	10.18 ± 3.82	8.26 ± 2.42	51.14 ± 24.40	43.71 ± 18.89

Supplemental Table-8: Individual subcomponents adjusted impedance summed, relative percentage of TB+ScP components in 1x and 1/10x PBS.

A) Sum of $Z^{AC}+Z^{ScP+TB}$ adjusted impedances

	bAdult			bCalf		
Freq.	**1khz**	**10khz**	**100hz**	**1khz**	**10khz**	**100hz**
PBS 1x	1,434 ± 40	1,416 ± 38	1,481 ± 33	3,322 ± 997	3,274 ± 993	3,367 ± 991
PBS 1/10x (2ml)	10,170 ± 6,078	9,785 ± 5,782	10,223 ± 6,136	-1,512 ± 407	-1,528 ± 401	-1,524 ± 421
PBS 1/10x (50ml)	9,042 ± 5,316	8,701 ± 5,059	9,158 ± 5,289	1,542 ± 560	1,489 ± 557	1,593 ± 582
	hNL			**hOA**		
PBS 1x	1,780 ± 531	1,748 ± 528	1,818 ± 529	1,584 ± 766	1,560 ± 748	1,587 ± 756
PBS 1/10x (2ml)	7,167 ± 4,186	6,884 ± 4,007	7,196 ± 4,198	7,177 ± 4,221	6,498 ± 3,608	6,724 ± 4,303

B) Relative percentages (ScP+TB/AC+ScP+TB) %

	bAdult			bCalf		
Freq.	**1khz**	**10khz**	**100hz**	**1khz**	**10khz**	**100hz**
PBS 1x	51 ± 1	51 ± 1	50 ± 1	76 ± 7	76 ± 7	76 ± 7
PBS 1/10x (2ml)	113 ± 25	115 ± 29	114 ± 25	30 ± 48	32 ± 48	32 ± 48
PBS 1/10x (50ml)	98 ± 5	98 ± 5	98 ± 5	54 ± 23	54 ± 24	54 ± 22
	hNL			**hOA**		
PBS 1x	99 ± 2	100 ± 2	99 ±2	100 ± 4	100 ± 3	100 ± 3
PBS 1/10x (2ml)	119 ± 13	120 ± 13	120 ±13	123 ± 17	124 ± 17	122 ± 16